CRACK DETECTION USING A PASSIVE WIRELESS STRAIN

SENSOR

A Thesis
Presented to
The Academic Faculty

by

Gabriel Lantz

In Partial Fulfillment
Of the Requirements for the Degree
Master of Science in the
School of Civil and Environmental Engineering

Georgia Institute of Technology
December 2011

CRACK DETECTION USING A PASSIVE WIRELESS STRAIN

SENSOR

Approved by:

Dr. Yang Wang, Advisor
School of Civil and Environmental Engineering
Georgia Institute of Technology

Dr. Roberto T. Leon, Co-advisor
School of Civil and Environmental Engineering
Georgia Institute of Technology

Dr. Manos M. Tentzeris
School of Electrical and Computer Engineering
Georgia Institute of Technology

Date Approved: August 10th, 2011

ACKNOWLEDGEMENTS

There were many people that have supported me during my studies at the Georgia Institute of Technology. I would particularly like to thank my thesis committee, Dr. Yang Wang, Dr. Roberto Leon and Dr. Manos Tentzeris. I would also like to thank all my lab mates. The discussions we had during the weekly meetings were also very interesting and intellectually constructive. A special thanks to my colleague, Xiaohua Yi, whose help and hard work have made my work easier. I am indebted to all the great teachers throughout my education who strengthened my curiosity in science. I would like to thank my family for being always there for me. I would also like to thank the southeast rock climbing community for helping me keep a balance between school and sports.

TABLE OF CONTENTS

LIST OF FIGURES

SUMMARY

Nearly one third of the 604,426 bridges in the United-States are either structurally deficient or functionally obsolete. Monitoring these bridges is essential to avoid catastrophic accidents. In steel bridges fatigue induced crack/rupture, which is one of the most common modes of failure, can be avoided if the crack is detected at the early stages of its formation. Cracks usually originate at stress concentration areas but their precise origin is random. Such strain concentration can be monitored with traditional strain gages, but their installation requires lengthy wires and equipment, which are expensive and labor intensive. Therefore wireless sensors are being developed to cope with these problems. In this work, a passive wireless strain sensor based on RFID technology is described. The sensor is a patch antenna that resonates at a certain frequency, which shifts in presence of strain. The relation between the resonance frequency and the strain is approximately linear. The slope of the relation is called sensitivity. The behavior of the sensor's sensitivity is studied using experimental work and simulations that couple electromagnetism and mechanics. The sensitivity measured in experiments and in simulations in presence of uniform strain is different. This difference is lower for the sensitivity in presence of a crack, probably due to a parameter variation that is currently not accurately modeled in the simulations.

CHAPTER 1

INTRODUCTION

1.1   Motivation

There are 604,426 bridges in the United States, of which 69,223 (11.5%) are structurally deficient and 77,395 (12.9%) are functionally obsolete [1]. Therefore structure health monitoring is essential to avoid catastrophic accident. In 2009, the annual spending in construction and maintenance of bridges was $10.5 billion whereas $17 billion investment would be needed [2]. With this budgetary constraint, structure health monitoring has to be inexpensive. Steel and aluminum iron bridges represent nearly one third of the total bridges but have a higher rate of deficiency than other types; 19.4% of these bridges are structurally deficient and 17.8% are functionally obsolete. Therefore monitoring these bridges is of particular interest. The most common cause of failure for steel bridges is fatigue-induce fracture/crack, where an early detection can both prevent the collapse of the entire structure and result in cheaper retrofits. Currently the biennial bridge inspections are mainly visual assessment [3]. However human labor is expensive and the human eye can easily miss cracks, especially if the inspection happens at the early stages of the crack growth or if the bridge has a paint coating. Routing highway bridge inspection can be unreliable and presents a high variability in the rating of bridge elements [4]. Finding new effective and inexpensive technologies to assist in structure health monitoring has become a priority in order to cope with the increase of deficient bridges and with budget cuts.

1.2   Background

Many technologies have been developed to answer the need of structure health monitoring. A typical structure health monitoring system consists of three modules as shown in Figure 1.1: (1) the sensor itself, which detects the change in condition (a crack,

for example), (2) the network that transmits the data, and (3) the data storage or computation center, which analyses the data.
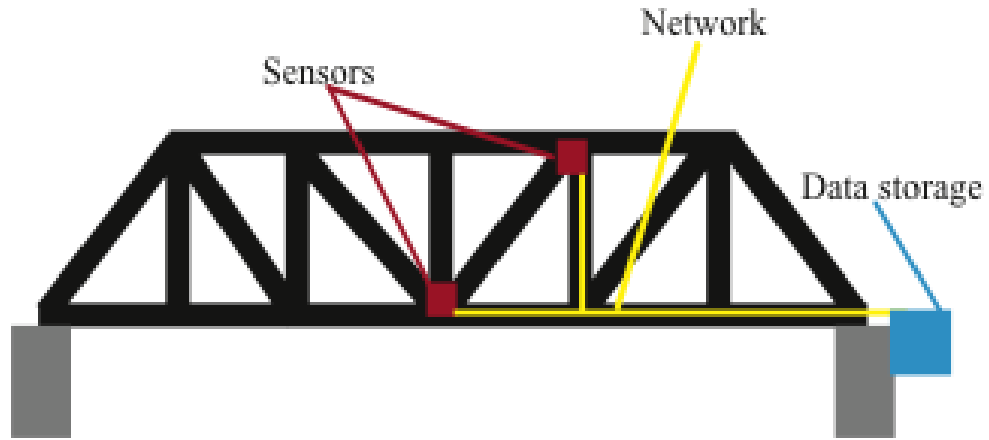
Figure 1.1: Typical scheme for a structural health monitoring system

A typical system uses metal-foil strain gages or accelerometers as the sensors, and the communication network is coaxial cables that link the sensors to the data storage center. According to Celebi [5], the cost per sensing channel for a mid-rise building is around $4,000. About half of the price of the system is labor cost due to the installation of lengthy cables. The Tsing Ma suspension bridge has a 600-channel monitoring system, which costs $16 million [6]. Therefore the first option to lower the price is to remove the cables by using wireless devices in the network. This type of communication network, called a wireless sensor network, has been developed mostly in recent years. Lynch et al. summarize the advances in this field in [7]. The sensor itself in a wireless sensor network typically has not changed; they are still typical accelerometers and strain gages, which are connected to the wireless node using short wires. Detecting damages in a structure can be done in two ways globally or locally. Global based damage detection identifies changes in the vibration modes of the structure and numerically determines if the structure is damaged globally [8]. Local based damage detection determines exactly where the damage is happening, for example, locating areas where active corrosion or points where crack propagation is occurring. Cracks typically originate at stress concentrations, one

can be predicted from experience in terms of triaxiality of stresses and local deformations. However the initiation of the crack occurs at material imperfections at the crystal level, which are random. In addition, initial crack growth is very slow and its direction unknown. Therefore large areas have to be monitored in order to detect the first initiation of the crack.

Several wireless sensor technologies have been developed in the past few years to address these problems. The basic concept of these sensors is to use the deformation of the base material to change the length of the sensor, which causes its behavior to change (i.e., its resonance frequency to shift or its electrical resistance to change). Because of the sensitivity of measurements based on electrical resistance or current to long-term stability and networking issues and because of their installation and maintenance costs, frequency shifts are a preferred approach today. For these sensors a relation between the resonance frequency and the strain obtained in the laboratory is used to determine the strain in the field from a measured frequency shift. A large variety of these sensors are available. For example, Chuang et al. have developed a wireless strain sensor that can be embedded or bonded in structures [9]. In this sensor, a cylindrical coaxial cavity of about 10 cm resonates at 2.45 GHz. The resonance frequency of the cavity shifts with changes in strain. The cavity is connected to an exterior antenna so that the interrogation can be done remotely. The cavity is more likely to be used inside concrete because of its cylindrical shape. Deshmukh and Huang used a microstrip antenna patch as the sensor mechanism [10]. The antenna is simply glued to a metallic surface; when subjected to strain, the antenna deforms and its frequency shifts. They report an approximate linear shift of resonance frequency due to strain [11]. Merilampi et al. also use the shift of the resonance frequency to detect strain [12]. The tag used is a printed RFID (radio frequency identification) dipole antenna of about 10 cm. Their results are more a proof of concept than a useful prototype. Using RFID technology, Sample et al. have developed a wireless identification and sensing platform (WISP), which can be connected to ordinary

metal-foil strain gages [13]. The WISP technology would work very similarly to a wireless node but it is smaller. Therefore many of these devices can be set up in a small area.

This thesis describes an RFID-based folded patch antenna to detect strain and cracks on metal surfaces. In presence of strain the length of the patch antenna changes causing the resonance frequency to shift. The linear relationship between the shift of the resonance frequency and the strain is called sensitivity. In order for the sensor to be useful for crack and strain detection, it has to fulfill certain criteria, as described in the next section.

1.3   Sensor requirements

For practical deployment of structure health monitoring, the sensor has to be low cost to enable local-based damage detection. The other requirements are size, accuracy and sensitivity characteristics. The sensor has to be small enough for it to be installed in areas where space is very limited, for example between two rivets. The sensor has to be accurate enough to detect a crack before the structure fails.

Inkjet-printing technology is a promising technology to reduce the cost of the sensor [14]. The antenna sensor is printed on paper using conductive ink, which would be inexpensive and allow mass production. These sensors can then be deployed in very large number on the desired surface.

Stress concentration areas have to be completely covered with sensors to detect a crack at the beginning of its formation. A sensor array can cover a very large area. If the sensors are installed with a grid pattern, there is a gap between each sensor. Therefore the crack can occur either between sensors (Figure 1.2) or go through a sensor (Figure 1.3).
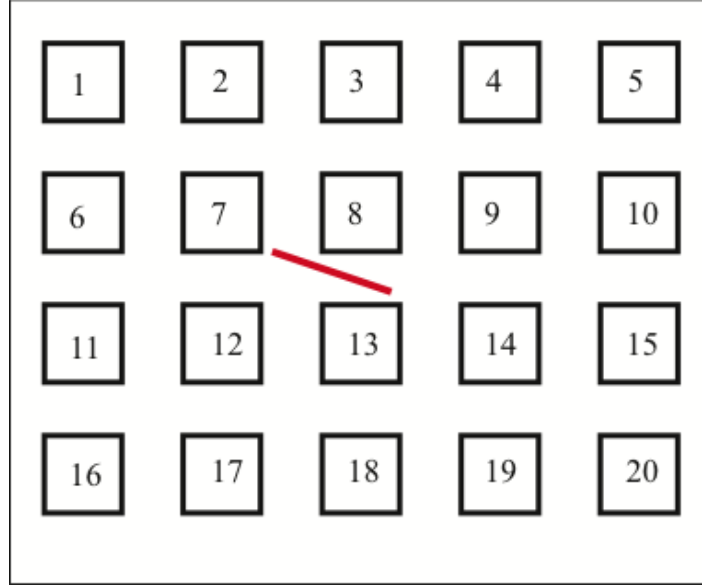
Figure 1.2: Sensor array with crack occurring between the sensors

Figure 1.2 shows a sensor array with a crack occurring between the sensors. The sensors are installed on a surface already under load, and therefore the sensor will pick up only additional changes in strain. The identification of the sensor helps to create a precise mapping of the strain. In the case of Figure 1.2, the sensors that undergo the most changes are number 7, 8, 12 and 13. A strain reference is needed in order to detect the change of strain. Because the strain is very localized near the crack [15], one possibility is to use the strain levels in the sensors that are far from the crack, for example number 5. The strain far away from the crack tends to be more uniform, therefore the behavior of the sensor in presence of uniform strain is important. Chapter 2 of this thesis will investigate the performance of the sensor in presence of uniform strain.

Figure 1.3 represents a case where the crack goes through a sensor. The sensor number 8 and 14 will be greatly affected by the crack. Chapter 3 examines the behavior of the sensor in close proximity of the crack or directly over the crack.
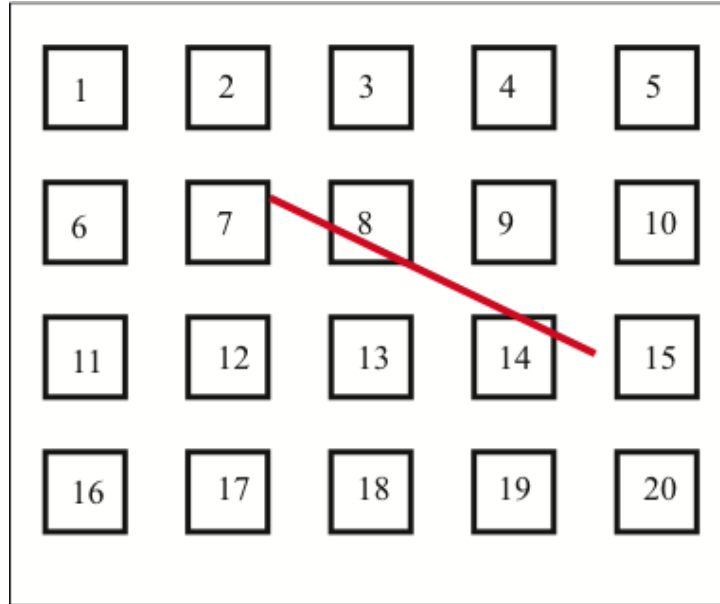
Figure 1.3: Sensor array with crack occurring through the sensors

1.4   Thesis organization

Chapter 2 presents the wireless sensor and a brief description of RFID technology concepts as well as experimental and simulation results for uniform strain. Chapter 3 investigates the performance of the sensor near a crack and on top of one using experiments and simulations. Chapter 4 summarizes the work and presents some possible improvements for the experiments and the simulations.

CHAPTER 2

RFID-BASED WIRELESS STRAIN SENSING

A wireless strain sensor was designed and fabricated using an RFID antenna as the sensing component [16]. The strain is derived from the shift of the antenna's resonance frequency. Simulations and experimental work are conducted on this innovative design. Section 2.1 presents the design of the sensor. The relationship between the resonance frequency shift and the strain is called sensitivity, and is investigated using experiments in section 2.2 and using simulations in section 2.3.

2.1   Sensing mechanism of RFID strain sensor

To obtain the precise location and direction of the cracks shown in Figures 1.2 and 1.3, each sensor must have its own identification. In our strain sensor, RFID tags are used to identify each sensor.

2.1.1   RFID principle

RFID tags are an electronic data storage system with a computational capacity. They are typically used as an identification system. Its power supply and data exchange are done via electromagnetic waves. An RFID tag is composed of two parts, the antenna and the IC (integrated circuit) Chip [17]. The antenna collects the energy from the electromagnetic waves, transmits it to the IC chip, which modulates it and reflects it back (backscatters it). An RFID reader is used to generate the electromagnetic waves and to demodulate the backscattered signal. Figure 2.1 represents one such typical RFID system. The reader interrogates the tag via an antenna. The IC chip is activated by the energy collected by the tag antenna and it reflects back the modulated signal to the reader. As the RFID tag does not have its own power supply, it is considered to be a passive device.
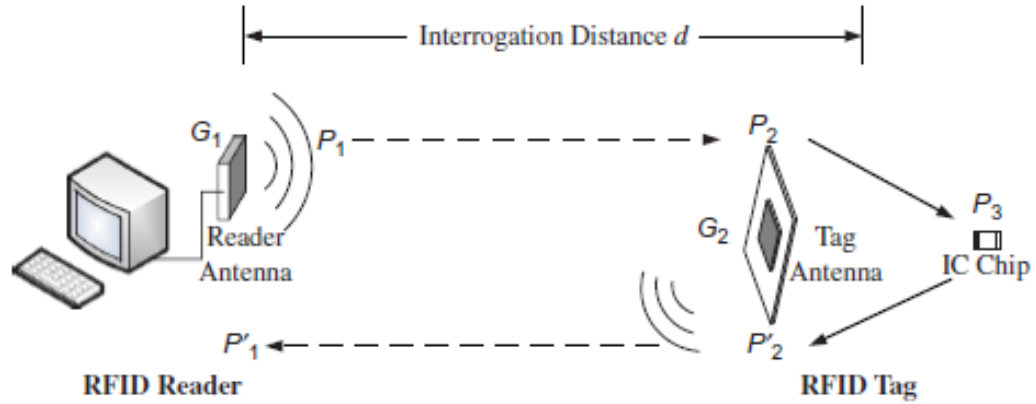
Figure 2.1: RFID system

The advantages of RFID tags are numerous. First of all, they are very cheap, at less than 10 cents per chip. Secondly they are passive therefore do not need any external power beside that provided by the reader, thus avoiding extensive wiring. Lastly they have an accurate identification system that enables a very large number of tags to be deployed in a very localized area.

For this work, the IC chip chosen was the SL3ICS1002 chip (manufactured by NXP Semiconductors) with an impedance of $13.3 - j122$ Ω (j is the imaginary number). It was selected for its low impedance that is easily matched to that of the tag antenna. The operating frequency range is from 840MHz to 960MHz, which allows international usage. The chip is connected to two large aluminum pads that enable an easy soldering. Figure 2.2 is a picture of the IC chip.
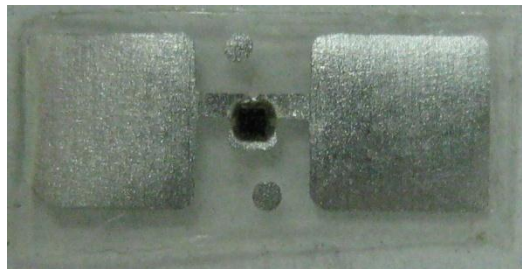
Figure 2.2: Picture of IC Chip

2.1.2   Patch antenna

As noted before, the RFID tag is composed of two parts, the IC chip and the antenna. The deformation of the antenna is responsible for the strain detection. Therefore the antenna is the most crucial part of the design. A quarter wave rectangular patch antenna (folded patch) design was chosen for two major reasons. The first one is its good performance on top of metallic objects, which is essential because the patch will be attached on metallic structures. The second reason is the reduced planar size of the patch that enables a better sensing localization. A regular patch antenna is a half wavelength in length while the folded patch is a quarter wavelength.

The patch antenna is shown in Figure 2.3 and described in [16]. The substrate is Rogers RT/Duroid 5880, which has a dielectric constant ε_r of 2.2 and a thickness of 0.79 mm. This substrate was chosen because it is made out of a glass polymer that does not micro-fracture. A good strain transfer from the bottom to the top of the sensor is necessary in order to have a similar strain behavior as the monitored structure. Consequently, a small thickness of the sensor is preferred. On the other hand, a small thickness reduces the antenna radiation performance. Therefore the thickness of the path is a tradeoff between the antenna performance and the strain transfer.

The antenna has two copper layers. The bottom side is the electronic ground plane, which will be glued to the surface of the monitored structure. The topside has the antenna design with IC chip connection. The two planes are electronically connected together by holes with copper in them called vias. The conducting material is a 17μm electrodeposited copper layer.

The IC chip is glued to the antenna with silver epoxy rather than solder because the quality of the soldering varies more and therefore changes the impedance. The long line that connects the IC chip to the patch is the matching network.
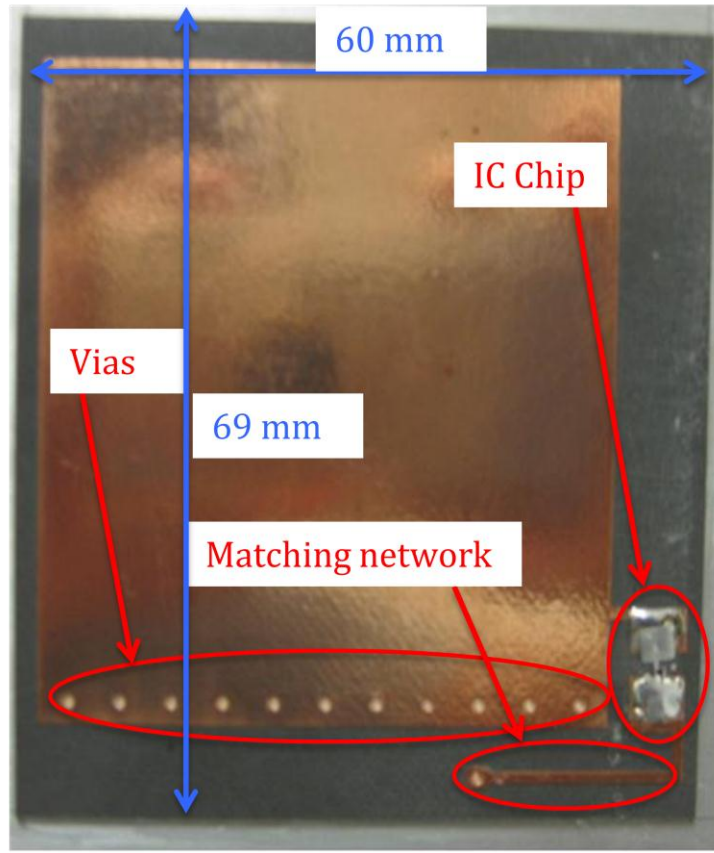
Figure 2.3: Picture of the RFID tag

An important parameter that characterizes the antenna performance is the resonance frequency. The theoretical formula for the resonance frequency of the folded patch antenna is:

$$f_{R0} = \frac{c}{4(L+L')\sqrt{\varepsilon_r}}$$ (2.1)

where f_{R0} is the theoretical resonance frequency under zero strain, c is the speed of light, L is the physical length of the antenna (54mm), L' is the additional electrical length due to the substrate thickness, and ε_r is the dielectric constant of the substrate. Since the substrate thickness is very small compared to the antenna length, L' can be approximated as zero.

The design of the sensor has to take into account the frequency bands used by telecommunication. The common RFID systems are built for the ultra high frequency range (UHF), especially between 800 MHz to 1 GHz. The cell phone band in the United States is GSM 850, which has a frequency band from 825 MHz to 894 MHz. Therefore the sensor is designed to have a resonance frequency around 915 MHz to avoid ambient noise from cell phones. In the future the sensor will need to be reduced in size to enable a more accurate localization of strain. To allow miniaturization, its frequency will be shifted to the super high frequency (SHF).

2.1.3 Deformation effect

In presence of strain the antenna's longitudinal length changes and the resonance frequency described by (2.1) becomes:

$$f_R = \frac{c}{4(1+\varepsilon)(L+L')\sqrt{\varepsilon_r}} \tag{2.2a}$$

$$= \frac{f_{R0}}{(1+\varepsilon)} \tag{2.2b}$$

$$\approx f_{R0}(1-\varepsilon) \tag{2.2c}$$

where ε is the strain experienced by the antenna. This equation shows that the shift in the resonance frequency is linearly related to the strain. Thus, strain can potentially be derived from the resonance frequency shift. The linear coefficient of the relationship between the resonance frequency and the strain is called strain sensitivity. From this formula the sensitivity should be f_{R0}. In practice, however, the actual sensitivity will be slightly different because of the approximations in the formula.

The sensitivity is found through a combination of experiments and simulations. Simulations help understanding the operation of the sensor in the presence of strain. There are two ways of simulating it. The first is simply by changing the dimension of the antenna using the longitudinal strain. This simulation gives an approximation of the

sensitivity. The second way is first using a mechanical simulation to obtain the deformed configuration under strain and then using the result to carry out an electromagnetic simulation. The second method should be closer to the experiment because it takes into account the non-uniformity of the strain distribution along the patch antenna.

In experiments the resonance frequency is found using the RFID system with a reader antenna (Figure 2.1). The resonance frequency originates from the best impedance matching between the tag antenna and the IC chip. Therefore the efficiency is maximum and the transmitted power needed to activate the IC chip is minimum. The minimum transmitted power needed to activate the IC chip for each frequency is called the transmitted power threshold. At the resonance frequency, the transmitted power threshold will be the lowest minimum. The RFID reader sweeps a frequency range and for each frequency it finds the minimum transmitted power necessary to have a response from the RFID tag.

Another approach to determine the resonance frequency is transmitting a constant power and recording the received power (backscattered power from the RFID tag). The received power would be maximum at the resonance frequency because the efficiency of the RFID tag is maximum at that frequency. The reader doesn't have to change the power and therefore the time required to sweep a frequency range is much faster for this method. The received power has values around -33 dBm and incorporates also a lot of ambient noise. Thus the signal is much more noisy and the determination of the resonance frequency is less accurate. The transmitted power threshold is less noisy because the transmitted power is more than 20 dBm and adding the ambient noise would not add a significant amount of power to activate the IC chip.

In the simulations, the reader antenna is not explicitly modeled for reasons dealing with length and complexity of the computations; so another parameter has to be chosen to characterize performance. The parameter chosen is the S11 parameter that corresponds to the return loss. It measures how much power is reflected from the antenna. The S11

parameter is measured at the IC chip and it varies from 0 to 1. If it equals 0 that means that the entire energy passes from the IC chip to the antenna and if it equals 1 the antenna does not radiate. The S11 parameter is usually expressed in the dB scale, S11dB=10log(S11). The frequency at which the S11dB reaches its minimum is the resonance frequency.

2.2 Tensile testing

In order to validate the strain sensing principles, uniaxial tensile tests are conducted. The resonance frequency is monitored in order to derive the sensitivity of the sensor.

2.2.1 Experiment setup for stain sensing

The RFID tag is glued to a 42 in. by 6 in. by 0.125 in. aluminum specimen using Super Glue from Super Glue Corporation. The sensor is placed 1 in. from the center of the aluminum and 5 conventional strain gages (FLA-2-23-3LT, Texas Measurements, Inc) are installed at 1 in. from the center on the other half of the specimen along the loading direction, as shown in Figure 2.4. The tensile test is conducted using a SATEC 22-Kip testing machine controlled by a force command. The force control gives a more stable strain in time because it compensates for the slipping that can occur between the grips and the aluminum. As the test is going to be run in the low elastic range, a deformation control command is not needed for safety.
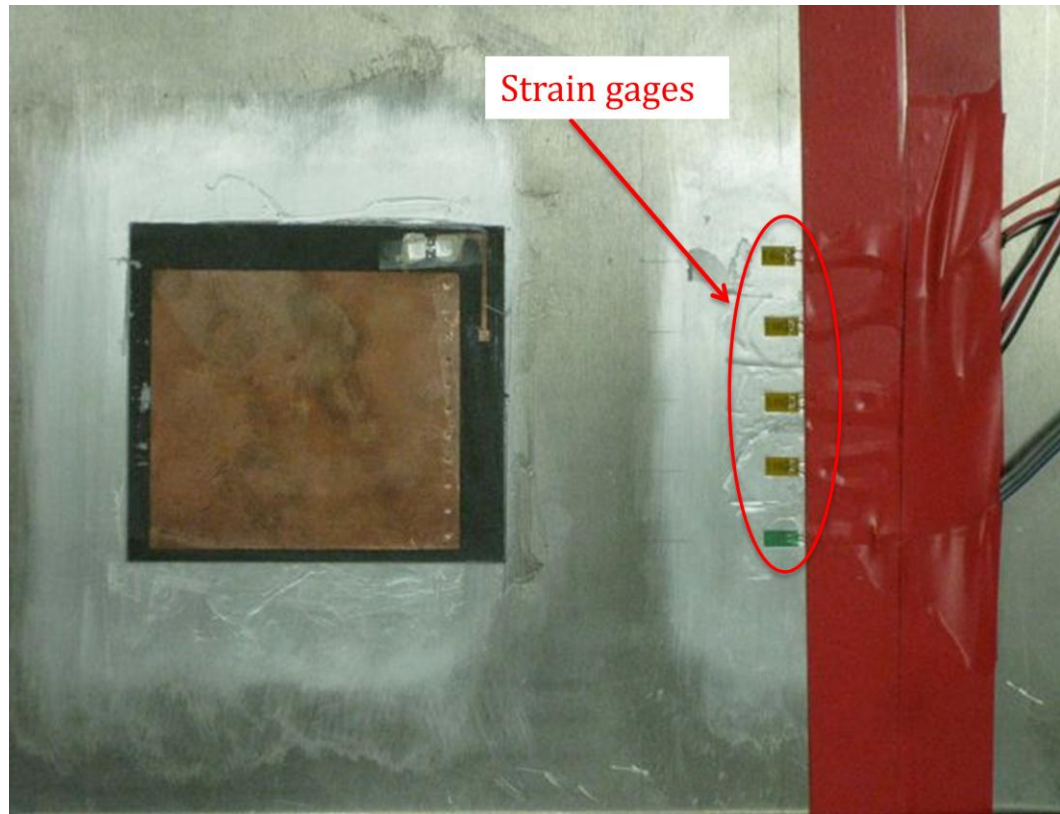
Figure 2.4: Wireless sensor glued on the aluminum specimen with strain gages

The transmitted power threshold is obtained using a Tagformance RFID reader manufactured by Voyantic. The frequencies are recorded every 0.1 MHz and the power measurement resolution is 0.1 dBm. The reader antenna is connected to the Tagformance with a coaxial cable and it is mounted on a tripod placed at 12 in. from the RFID tag. Figure 2.5 shows the picture of the experimental setup. The strain gages are connected to a National Instruments strain gage module (NI 9235), in combination with a CompactDAQ Chassis (NI cDAQ-9172) used for collecting strain gage data. The Tagfomance and the CompactDAQ Chassis are connected to a laptop through a USB 2.0 cable.
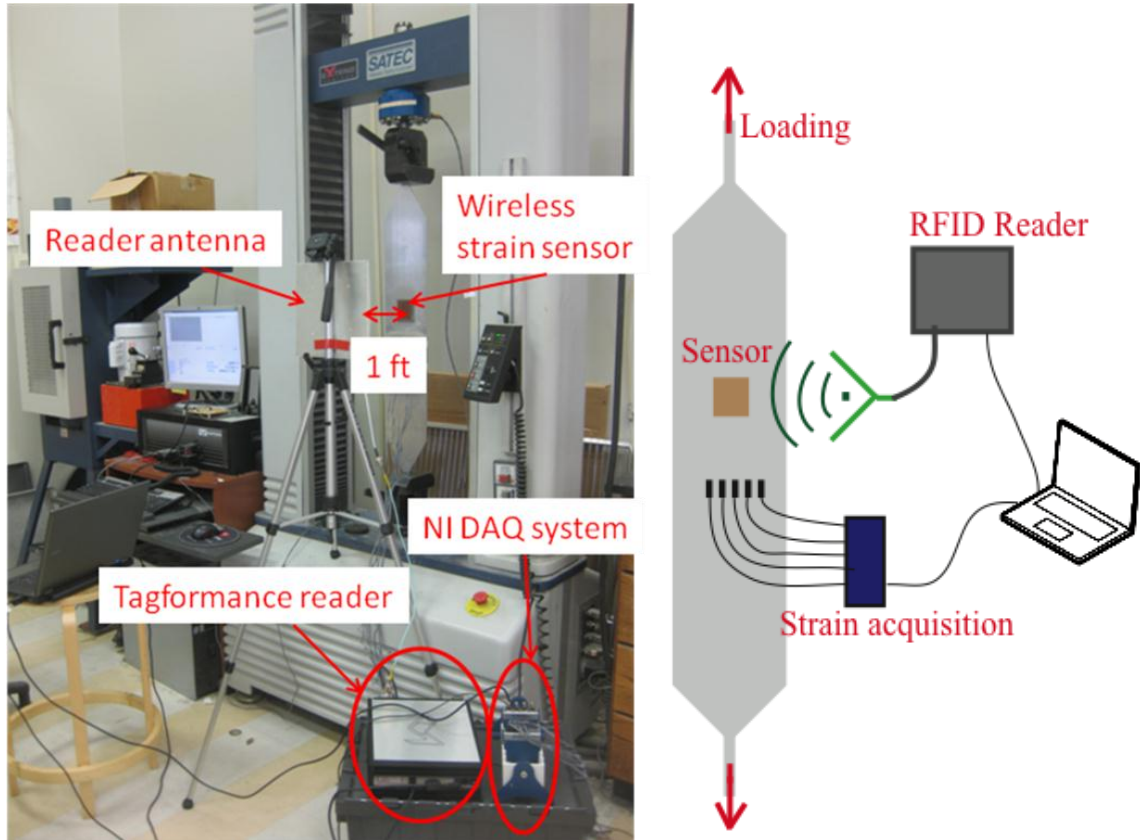
Figure 2.5: Experimental setup

2.2.2 Strain sensing results

The aluminum specimen is loaded at approximately 20 με per step. In order to reduce the noise in the data for each step, five frequency sweeps are done. At each frequency, the five measurements are averaged. Figure 2.6 represents the average transmitted power threshold for each strain step. The resonance frequency for zero strain is between 921 and 922 MHz.
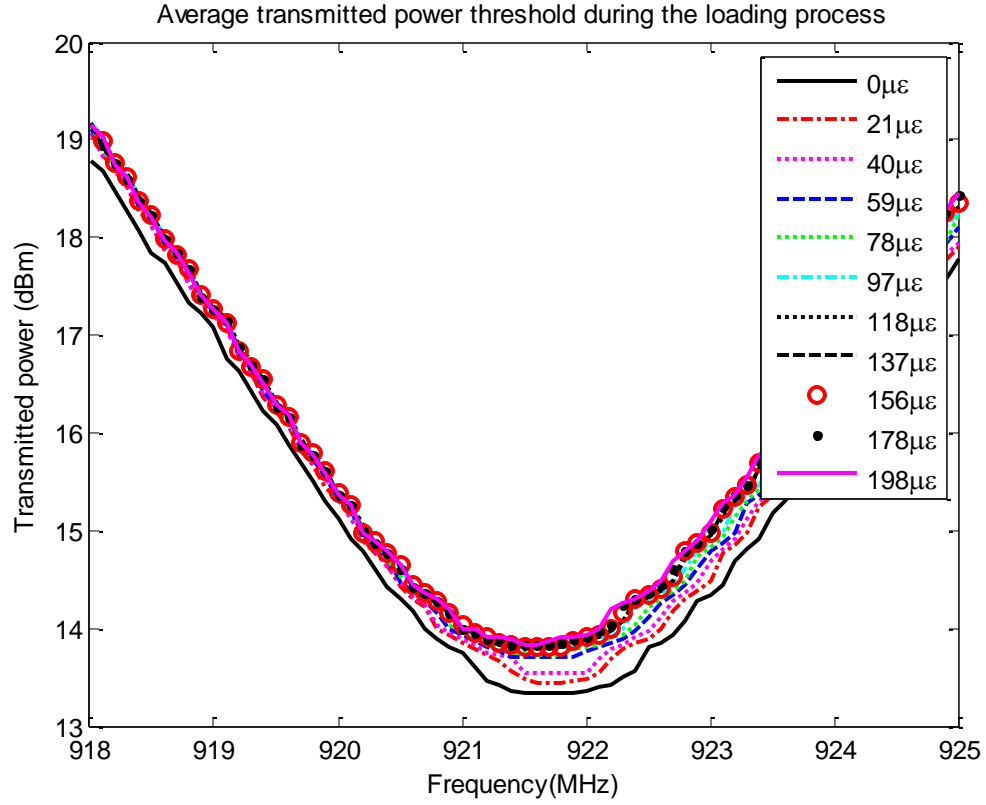
Figure 2.6: Average transmitted power threshold for loading process

The curve is not very smooth and doesn't have a precise minimum. Therefore a fourth order polynomial curve fitting method is applied on the central part of the curve, which is defined by all the points that are less than 3 dB away from the lowest point. Figure 2.7 shows the curve fitting method for zero strain level.
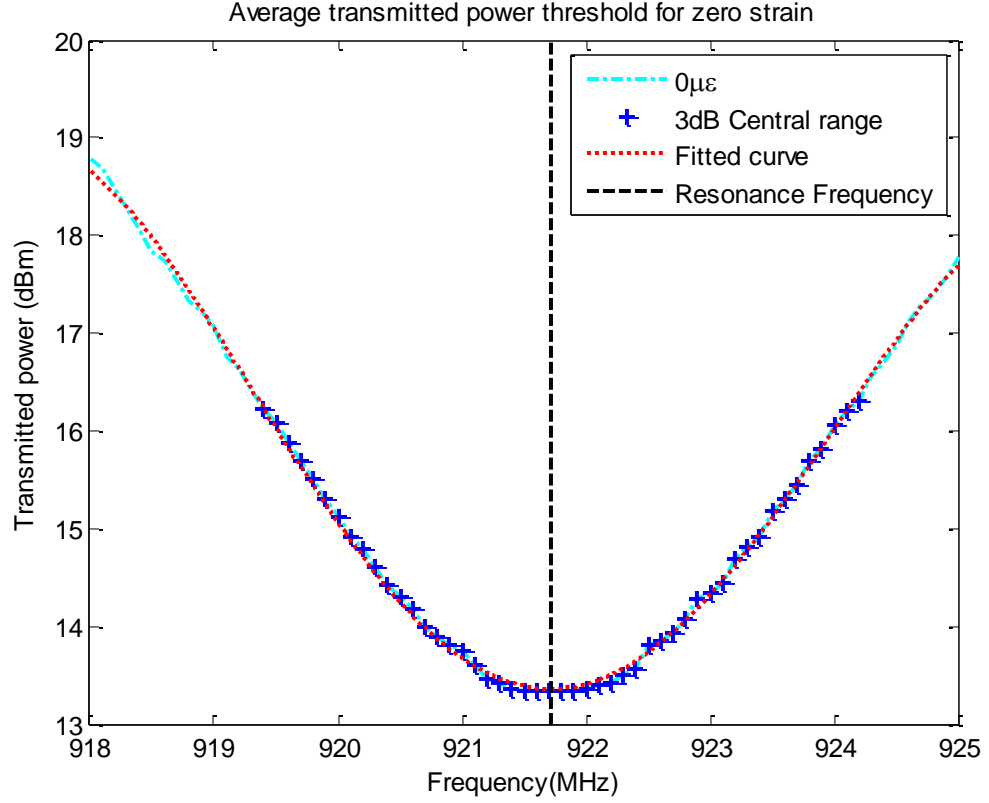
Figure 2.7: Curve fitting for zero strain level

The resonance frequency is then read by taking the minimum of the fitted curve. The resonance frequencies for each step are shown in Figure 2.8. A simple linear regression is conducted on the data points. The equation is of the form:

$$f_R = \beta_0 + \beta_1 \varepsilon + \delta \tag{2.3}$$

where β_0 is the intercept, β_1 is the slope (sensitivity), and δ is a random variable called random error term, $\delta \sim N(0,\sigma^2)$ is assumed.

In this regression, the estimated intercept is β_0=921.714MHz and the estimated slope (sensitivity) is β_1=-639Hz/$\mu\varepsilon$. The coefficient of determination R^2 is a number between 0 and 1 representing the quality of the linear fit. For a perfect linear relationship, R^2=1. The value R^2=0.9828 obtained experimentally represents a very good linearity.
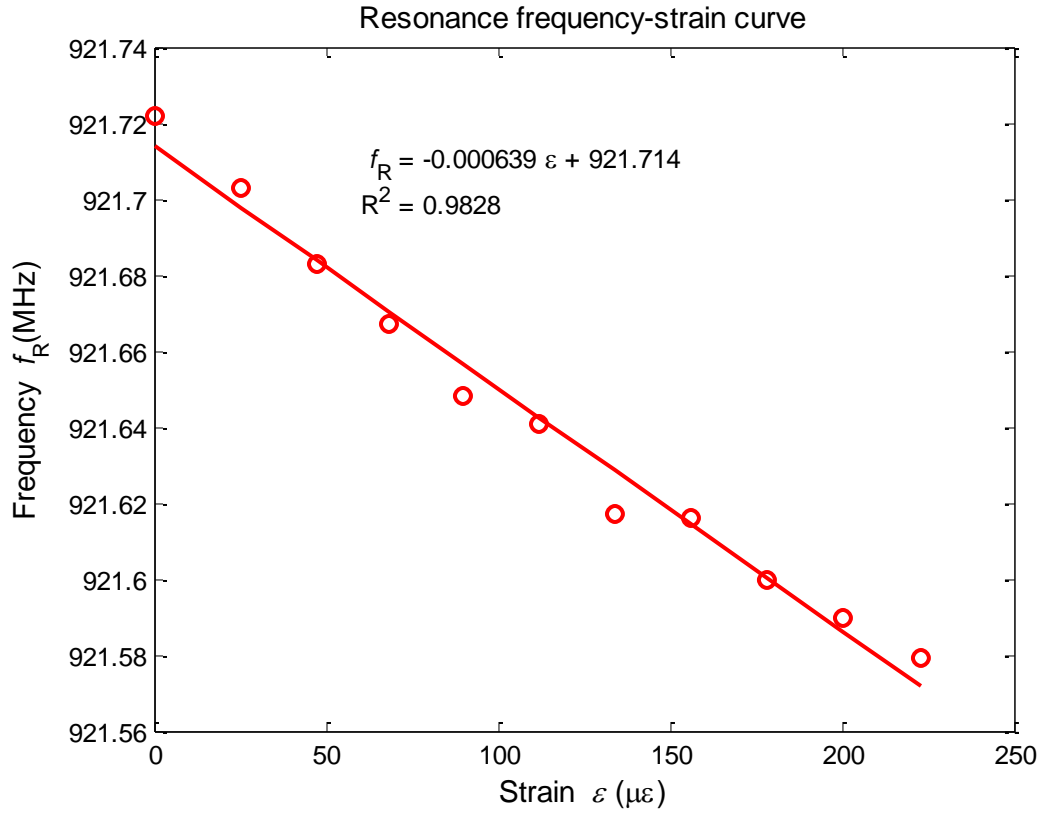
Figure 2.8: Resonance frequency f_R versus strain ε

The linearity is not perfect because of noise. Forty frequency sweeps were taken at zero strain to evaluate the noise level. Figure 2.9 represents the forty curves with the average in red.
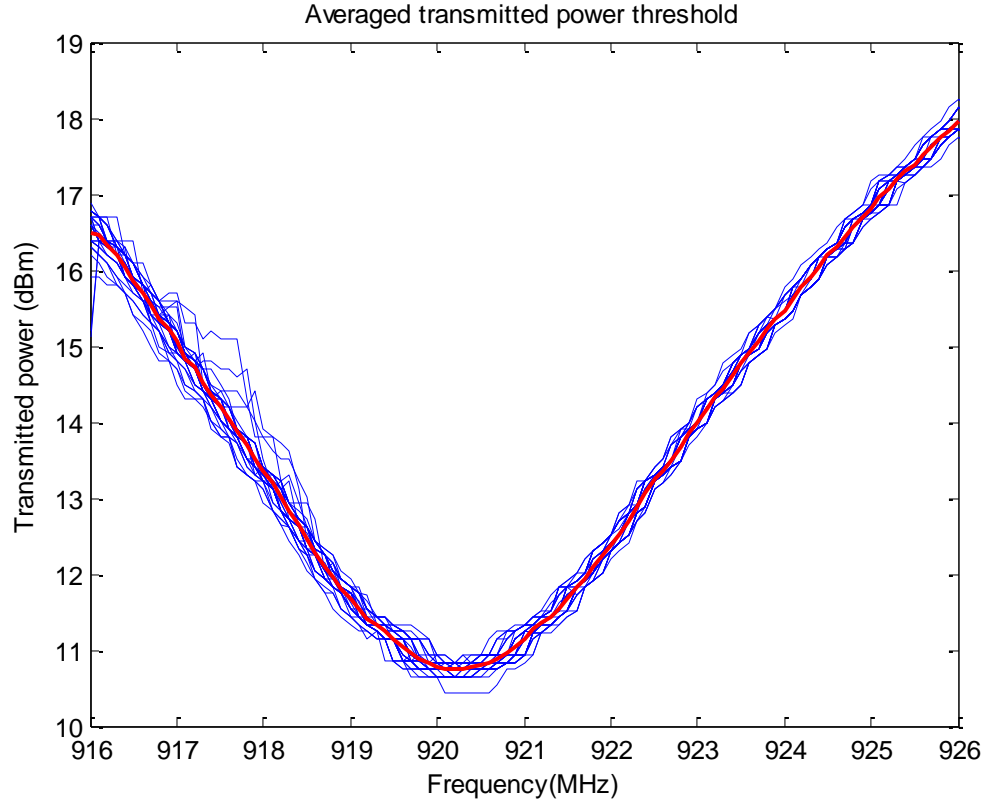
Figure 2.9: Transmitted power threshold for zero strain

Each curve was fitted with a fourth degree polynomial. The minimum of this fitted curve was peak picked. The standard deviation of these resonance frequencies is SD=0.0428MHz. To understand the distribution, the values are normalized and the Q-Q plot is shown in Figure 2.10, which plots the sample quantiles versus the standard normal quantiles. A linear plot means that the sample distribution is close to a normal distribution.
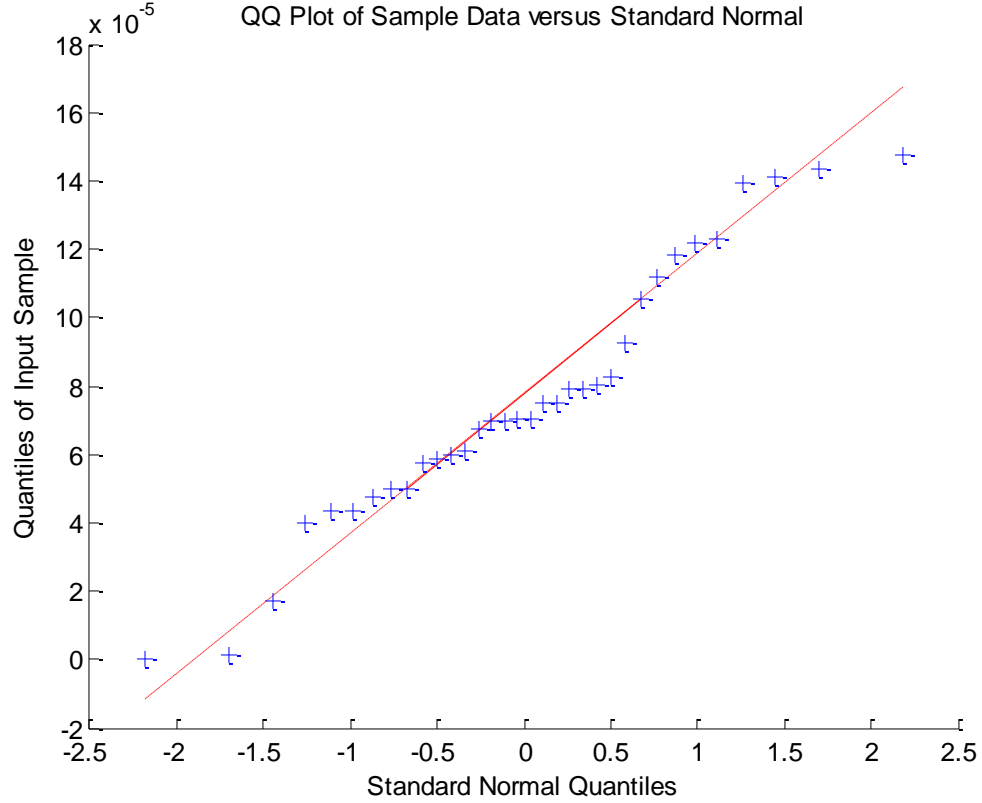
Figure 2.10: Q-Q plot of the 40 resonance frequencies

The Q-Q plot shows that the data is close to a normal distribution; therefore averaging the data m times will divide the standard deviation by square root of m.

In the tensile test described above the five curves are averaged to find the peak. The standard deviation of the averages is $SD_5 = \dfrac{SD}{\sqrt{5}} = 0.019 \, 1MHz$. This noise level plays a role in all data collection, whether it is in the sensitivity determination or just in shifting the measurement.

From more recent experiments, it is also clear that the resonance frequency is very sensitive to the temperature. Taking into account any small temperature shift could reduce the noise level.

2.2.3 Strain transfer

The patch antenna has a thickness of 0.79 mm. Therefore the strain on the aluminum is not the same as on the top copper of the sensor. The ratio between the strain on the top copper and the aluminum is called strain transfer. This parameter measures the correct behavior of the sensor. If the strain transfer is low, the sensitivity can be much lower than the theoretical estimation. The strain transfer ratio is validated experimentally. A piece of substrate Rogers RT/Duroid 5880 with similar dimension as the patch antenna is installed on an aluminum specimen. Figure 2.11 shows nine strain gages (#1-#9) installed on top the substrate. Six other strain gages (#10-#15) are installed near the center of the aluminum to measure the axial strain on the aluminum.
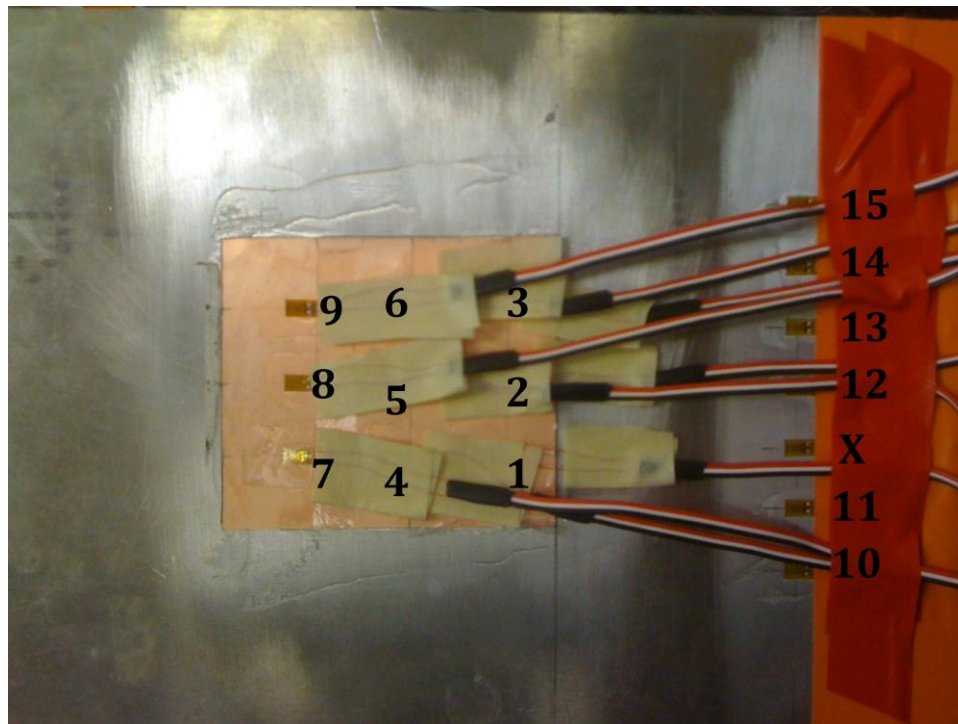
Figure 2.11: Picture of strain gages for the strain transfer experiment

The average reading from strain gages #1 to #9 give the axial strain on top of the substrate and the average reading from strain gages #10 to #15 is the axial strain of the aluminum specimen. The X between gage #11 and #12 means that the strain gage failed.

The ratio between the two averages is the strain transfer percentage. The specimen is loaded up to 400με at 10με per step. Figure 2.12 shows the strain transfer percentage for each strain step. The strain transfer converges to 90%. The low strain transfer at the beginning is likely due to the nonlinearity of the super glue. As soon as the strain reaches 50με the strain transfer is above 70%, which is very acceptable.
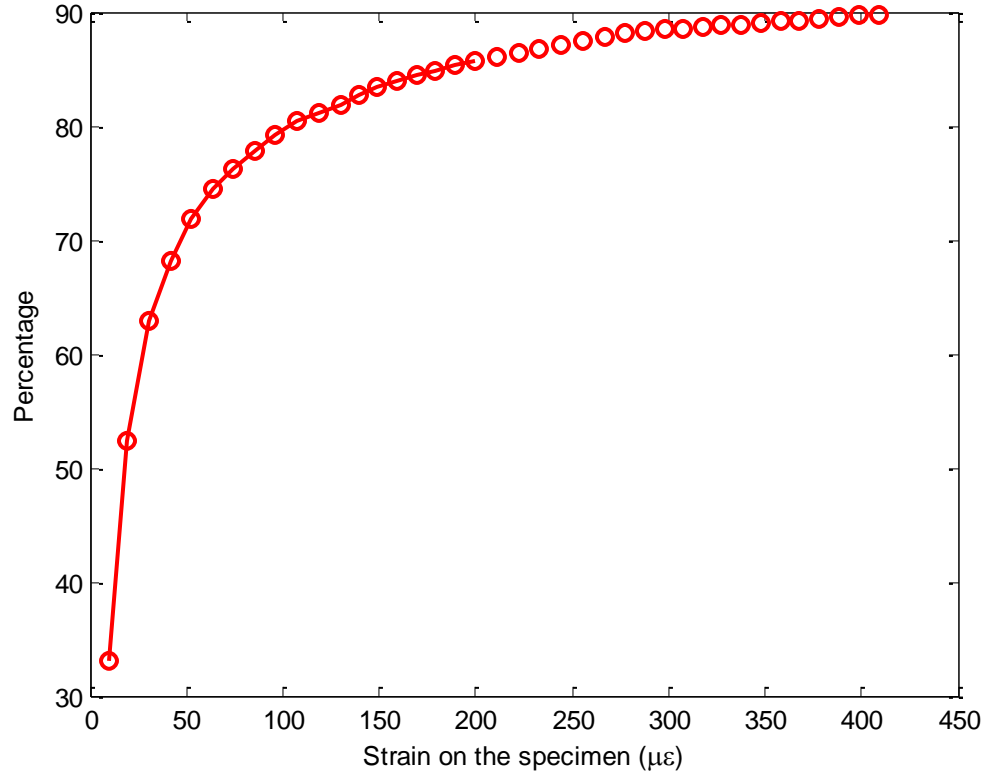
Figure 2.12: Strain transfer percentage for each strain level

Using the strain transfer data, it is possible to calibrate the results obtained in Figure 2.8. For each step, the strain is multiplied by its corresponding strain transfer ratio.

$\varepsilon_i` = \varepsilon_i \times st_i$

where ε_i is the strain of the ith step, st_i is the strain transfer ratio of the ith step, and $\varepsilon_i`$ is the new strain for the ith step.

Figure 2.13 shows the calibrated results. The sensitivity is now -724Hz/μɛ; this sensitivity corresponds to the case where the strain is directly measured on the top copper.
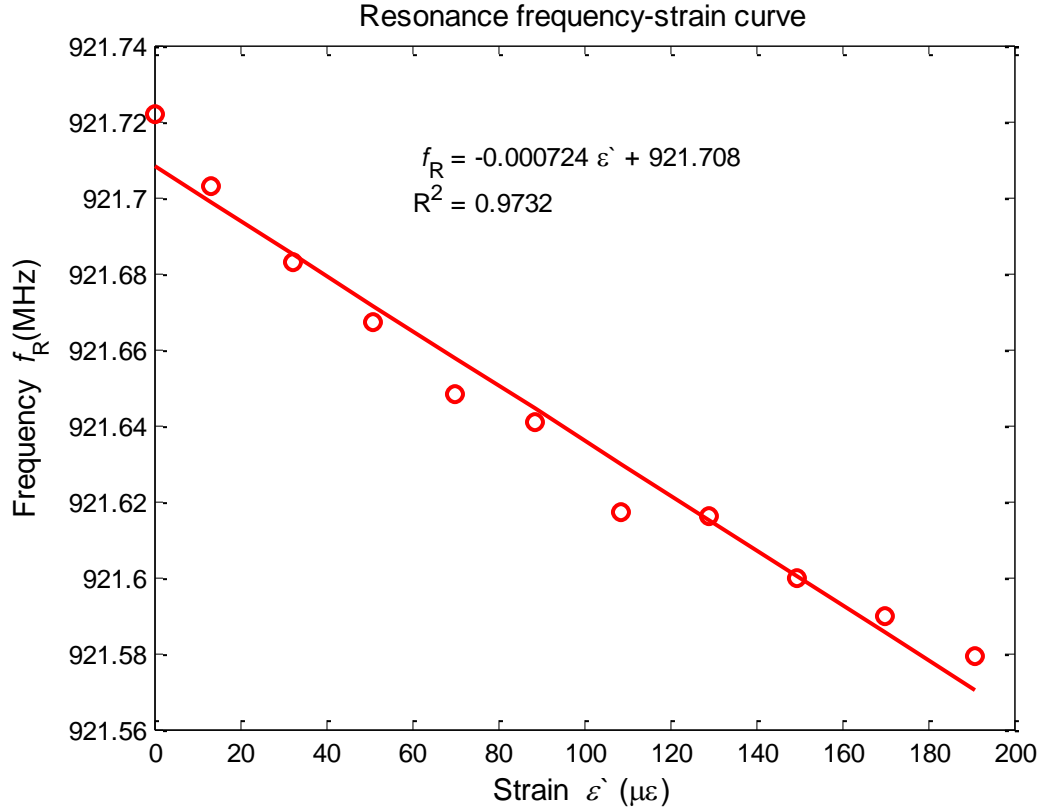
Figure 2.13: Resonance frequency f_R versus strain ε` calibrated with strain transfer data

Calibrating the data with the strain transfer is useful to understand the impact of the non-uniformity of the strain. For example if plastic deformation arises, the strain transfer decreases. Although the value of the calibrated sensitivity is closer to the theoretical value, it is still 22% lower. A possible explanation of this difference could be the variation of the dielectric constant of the substrate ε_r with the strain ε. Before making this assumption, coupling simulations between mechanics and electromagnetism are necessary to make sure that this difference doesn't come from a mechanical source.

2.3   Mechanical-Electromagnetic coupling simulation

The design of the sensor was initially done by simulation using HFSS, an electromagnetic field finite element simulation software. Unfortunately this software does not contain a mechanical module to simulate the exact strain in the sensor. COMSOL Multiphysics is especially design to handle coupled phenomena. Therefore it was selected to simulate the coupling between the mechanical deformation and the electromagnetic field. The simulation process is done in three parts. Each type of physics is simulated independently and tuned to fit the experimental data. First, for the electromagnetic simulation, the resonance frequency is matched to the one given by HFSS and the experimental results. Second, the mechanical simulation is carried out, with the strain transfer used to compare the simulation and the experiment. The final part is the coupling between the electromagnetic and the mechanical simulations, where the sensitivity is computed and compared to the experimental sensitivity.

2.3.1   Electromagnetic simulation

The first part of the simulation is to define the geometry. When building the geometry, it is important for computational time purposes to simplify the model by reducing the number of mesh elements. The simulation model is the patch antenna on an aluminum plate. COMSOL has two main categories of geometric objects: (1) surfaces that are meshed with two-dimensional elements, and (2) solid elements, which are volumes with boundaries that are surfaces. Solid elements are meshed using three-dimensional elements.

The aluminum is modeled by a solid element, which is a volume that is meshed using volume mesh elements. The dimensions of the aluminum are 120x163x3.17 mm, which are big enough to avoid side effects in the mechanical simulation and small enough to limit the number of mesh elements added. The substrate is also modeled by a solid element with the dimension of the substrate of the tag antenna. In the prototype the

copper layers are 17 μm thick. If a solid element was used, the mesh required would be very fine because the mesh elements have to be approximately the same size in each direction. Therefore the copper layers are modeled by surfaces, which are meshed by surface elements. Moreover the current distribution at the operated frequency is limited to the very top part of the copper surface. The penetration depth of the current is given by the skin effect equation, [19]:

$$\delta_s = \sqrt{\frac{1}{\pi \cdot f \cdot \mu_0 \cdot \sigma}} \tag{2.4}$$

where δ_s is the penetration depth of the current, f is the frequency, μ_0 is the permeability constant, σ is the conductivity of copper. The skin depth for the copper in the sensor is 2.18 μm, which is much smaller than the copper thickness. The vias are the smallest elements and are cylindrical, therefore are the most sensitive part of the geometric model. Curved elements are hard to mesh because they have to be approximated by lines. As the cylindrical shape of the vias is not essential for the electromagnetic simulation, they can be modeled by a parallelepiped, which is easier to mesh. The position of the vias in the y direction is very important because this controls the value L in equation (2.1), and consequently the resonance frequency. The resonance frequency can be tuned using this length. The design frequency is 915 MHz so the via position is select to be close to 915 MHz. Figure 2.14 represents the antenna geometry.
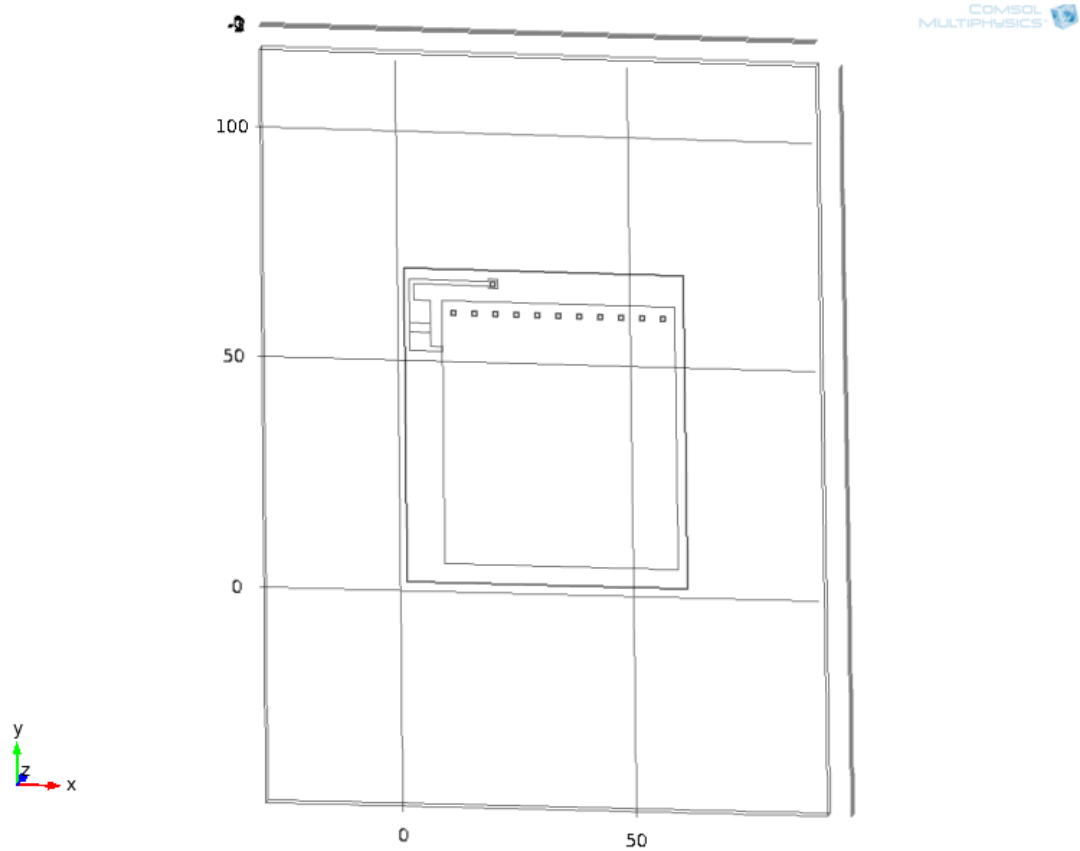
Figure 2.14: Antenna geometry for COMSOL simulation

The next step is to create the air around the antenna. Since it is impossible to model the whole environment, it is necessary to create a domain where the electromagnetic waves are absorbed and are not reflected. This domain is called perfectly matched layers (PML). In COMSOL, the PML are solid elements and not boundary conditions. Two spheres are built. The z coordinate of the center is on xy plane at the interface between the substrate and the aluminum. The x and y coordinates are at the middle of the antenna. The inner sphere has a radius of 150 mm and the outer sphere a radius of 186 mm. The region between the two spheres is the PML. The inner sphere is filled with air. PML regions have to be meshed using a swept method for smooth absorption. The swept mesh creates a mesh by building the mesh layer by layer from the source surface along the domain to the opposite destination surface. In order to apply this mesh, the domain has to have one

source face and one destination face. When creating a sphere in COMSOL, the outer surface of the sphere is composed of 8 sub surfaces, each an eighth of the sphere's surface. The region between the spheres is only one domain but has eight sub surfaces, and as such, it is impossible to use a swept mesh. Therefore the domain has to be cut into eight separate sub domains to be able to mesh it correctly. Workplanes are used to cut regions and do not interfere with the physics. Three perpendicular workplanes are created to coincide with the sphere's surfaces. One of the planes is on the interface between the substrate and the aluminum, if the center of the spheres would have been in the center of the substrate, this plane would have cut the substrate in two and dramatically increased the number of mesh elements. Figure 2.15 shows the whole electromagnetic geometry.
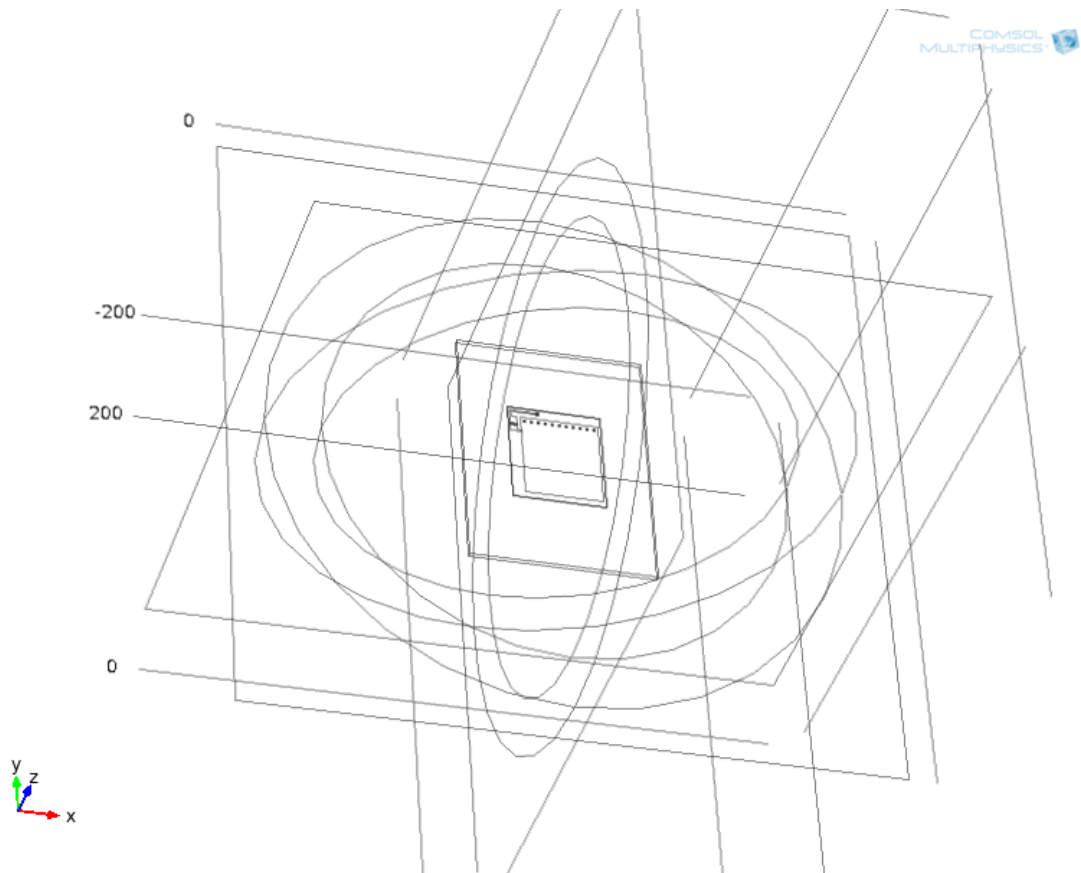

Figure 2.15: Electromagnetic geometry, sensor on aluminum with PML layers

Once the geometry has been built, it has to be meshed. The mesh defines the degrees of freedom, a finer mesh gives a better result accuracy but is more computational demanding. The maximum size of the mesh has to obey Nyquist rate [20], which says that the maximum spacing between two points has to be less than $\lambda/2$. The frequency is 915 MHz, therefore $\lambda=c/f=0.33$ m, so the smallest distance has to be 160 mm. The size is defined as normal with a maximum element size of 45 mm. First the sensor is meshed, using an automatic mesh with tetrahedron elements. Then the aluminum and the air around are meshed using the same tetrahedron elements Finally the PML region is meshed using a swept mesh with quadrilateral elements.

The next step is defining the material properties. The air, the copper and the aluminum have their properties already defined in the built-in COMSOL material library. The substrate material Rogers RT/Duroid 5880 is not built-in, and, its properties are defined using the data sheet of the product. The material properties used in the electromagnetic simulation are the dielectric constant ε_r, the relative permeability μ_r, and the electrical conductivity σ.

The electromagnetic properties are defined in the electromagnetic wave physics section of COMSOL. The eight PML regions are defined as a spherical wave PML setting with the same center as the spheres. The copper layers are modeled by perfectly electric conductors (PEC), which are conductors with no resistivity. Copper resistivity is very close to zero so this approximation does not appreciably affect the results. The reason to use PECs is that their behavior is simulated much faster. The excitation of the antenna originates from the IC Chip, which has an impedance of $13.3 - j122$ Ohm (where j is the imaginary unit). The IC chip is modeled by two lumped ports separated by a PEC surface. A lumped port is a surface with a specified impedance, which can have an excitation wave. The first lumped has an impedance of 13.3 Ohm and is excited by an input of 1 V. The second surface has an impedance of –j122 Ohm and the excitation is

off. Because these two ports are in series the global impedance is the addition of the two separate impedances and overall models well the IC Chip.

To verify the model, a simulation with only the electromagnetism is done. The solver used is a frequency domain solver, where a frequency range and a frequency step are specified. For each frequency, the solver computes a stationary problem with the specified frequency that computes the electromagnetic field E. An iterative method or a direct solver can compute the stationary problem. The direct solver inverts directly the matrix while the iterative solver finds the solution step by step with approximations. The direct solver works better in this case. The S11 is observed at the lumped port in order to find the resonance frequency. The resonance frequency occurs at the point when the S11 reaches its minimum because the impedance matching optimized at that frequency. First a coarse sweep with a step of 1 MHz is done around 915 MHz in order to locate the resonance frequency. Afterwards, a finer sweep is performed with a step of 50 KHz. Figure 2.16 shows the S11dB for the model with only the electromagnetic simulation, which is the reference for zero strain. The resonance frequency shows a clear peak at 920.5 MHz. The S11 at the resonance frequency is less than -10dB, which indicates a good matching.
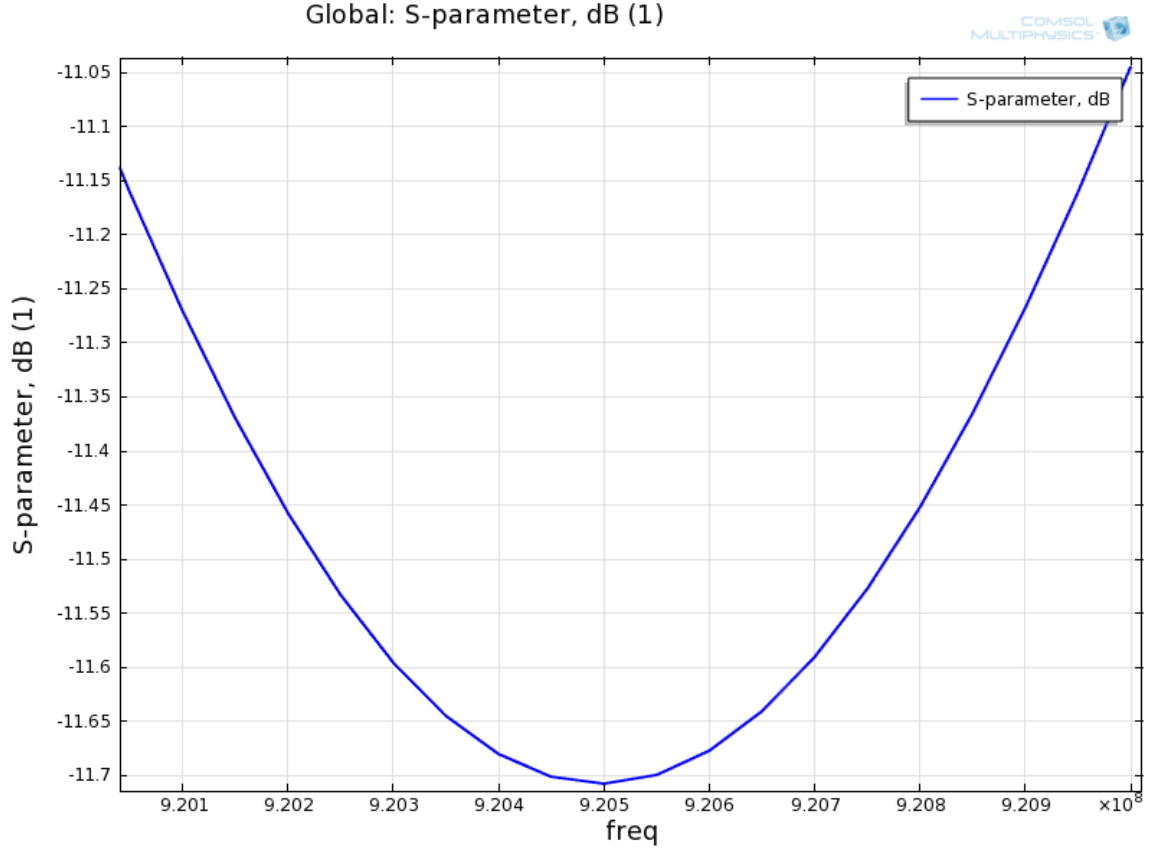
Figure 2.16: S11 for the electromagnetic model at 0 με

Increasing the length of the top copper without changing the dimension can give a first approximation of the sensitivity. The added length ΔL is appended on the opposite side of the vias. Once again, only the electromagnetism is simulated. Figure 2.17 shows the S11dB for a copper addition equivalent to 1000 με. The peak is at 919.3 MHz. The shift is -1.2 MHz for 1000 με, which corresponds to a sensitivity of -1200 Hz/ με. Using equation (2.1), theoretical shifting can be calculated:

$$f_R - f_{R0} = \frac{c}{4(L+L'+\Delta L)\sqrt{\varepsilon_r}} - \frac{c}{4(L+L')\sqrt{\varepsilon_r}}$$

(2.5a)

$$= \frac{3\times10^{11}}{4(54.5+0.414+57\times0.001)\sqrt{2.2}} - \frac{3\times10^{11}}{4(54.5+0.414)\sqrt{2.2}}$$

(2.5b)

$$= -954{,}790 \text{ Hz}$$

(2.5c)

Therefore the simulation result is 20% different from the theoretical results.

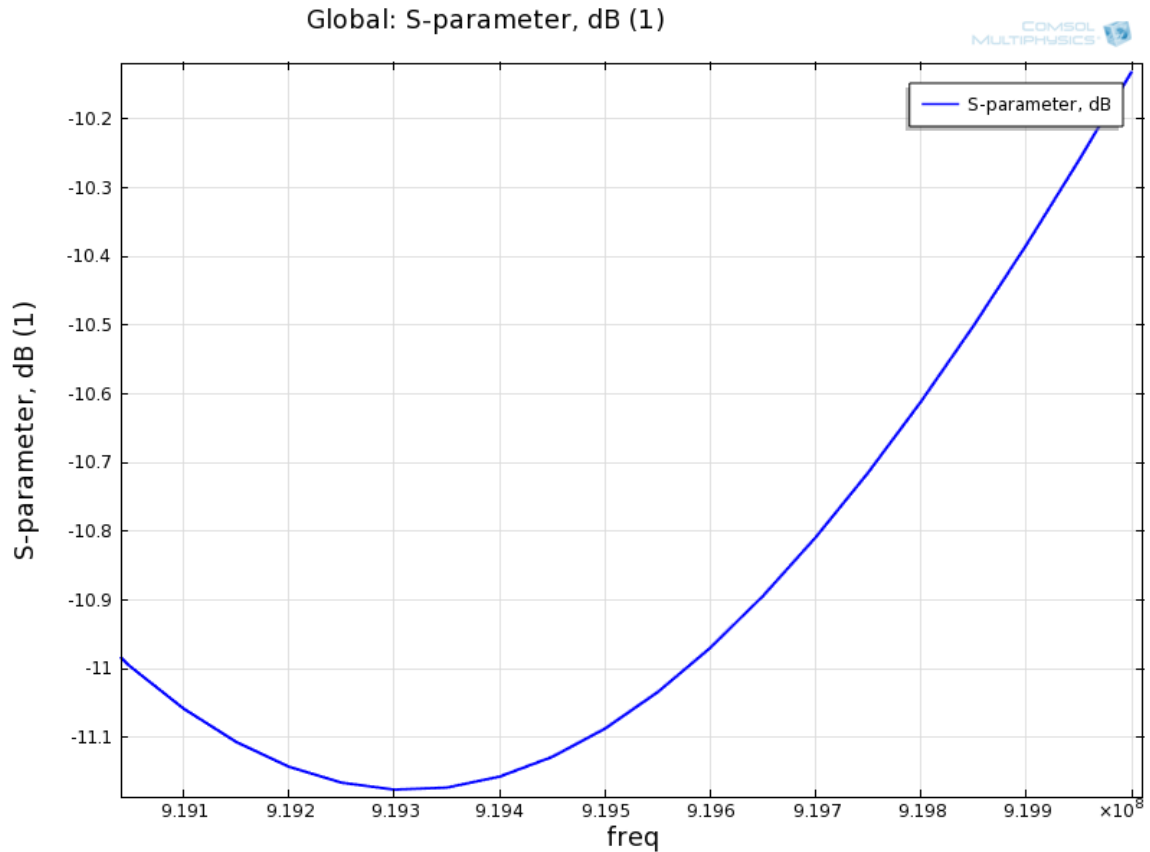**Figure 2.17:** S11 for the electromagnetic model with added copper corresponding to 1000 µε

2.3.2   Mechanical simulation

The mechanical simulation uses the same geometry and meshing as the electromagnetic simulation but without the air. Mechanical solids model all the volumes and shell elements model the copper surfaces. Shell elements are used to model a thin layer in three-dimensional structures. An artificial thickness of 17µm is given to derive the strength of the element. In the mechanical physics section, all the surfaces are free of deformation and load; only the two ends of the aluminum have an imposed displacement. The two displacements are along the y direction; the x and z displacements are set to zero to make the model mechanically stable. The displacements are chosen to give 1000µε,

and it is important that they are symmetrical in order to keep the sensor in the middle of the spheres. The simulation is a stationary problem with a fully coupled solver between the shell and the solid mechanics. A direct solver is used to compute the displacement field U for this simulation because it is faster than the iterative solver. In COMSOL versions 4.1 and 4.2, the solid mechanics module uses a moving mesh, which is a mesh that moves with the deformation. Fig 2.18 shows the strain in the y direction.
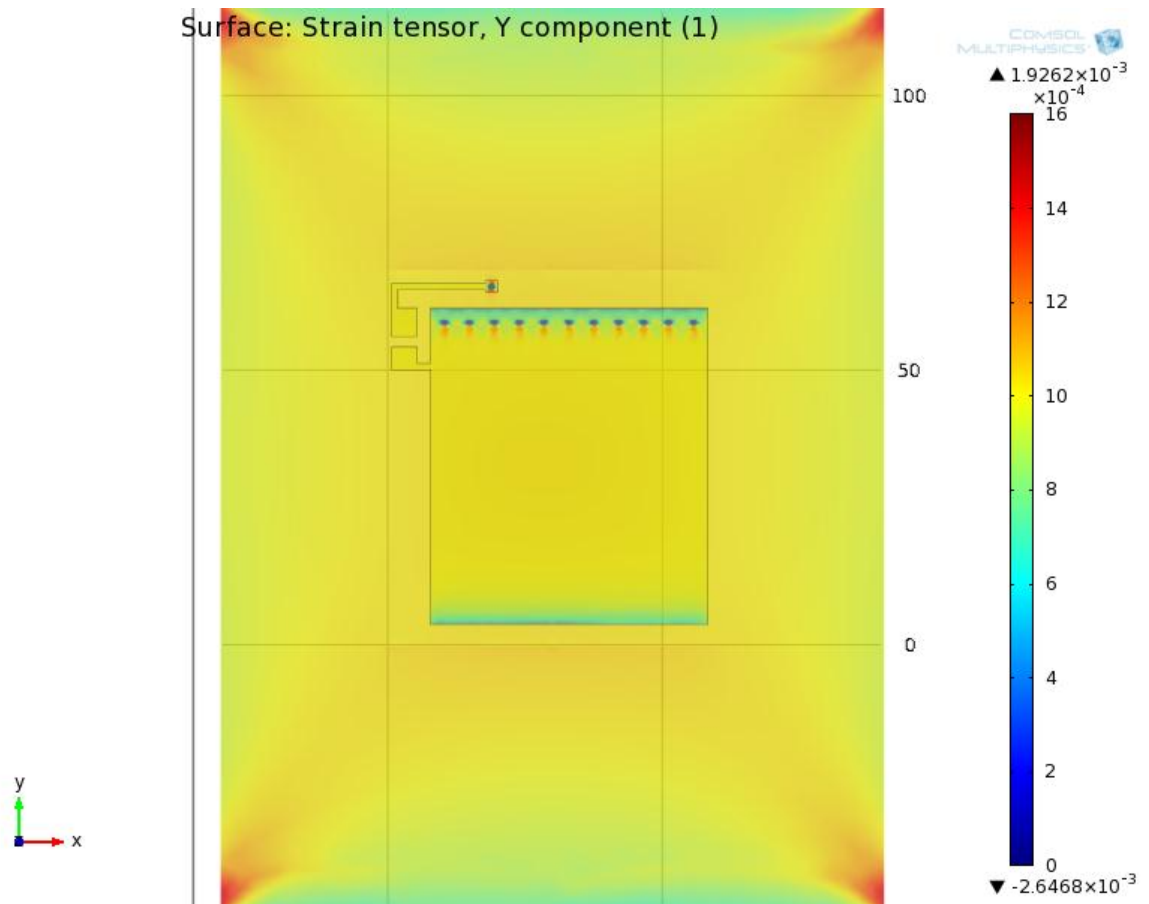

Figure 2.18: Strain in the y direction on the aluminum and on the antenna

The strain transfer is calculated using the average strain in the y direction on the top copper divided by 1000 με. The strain transfer value is 92%, which is very close to the experimental results from Figure 2.13.

2.3.3 The coupling simulation

The electromagnetic and the mechanical simulation work well separately. The aim of coupling simulation is to use the deformed configuration from the mechanical simulation as an input for the electromagnetic simulation. There are three ways of building the coupling in COMSOL. The first is the export/import method, which exports the deformed configuration of the sensor and the aluminum from the mechanical simulation and imports it into the electromagnetic simulation. This method isn't very precise because the exporting process is not accurate enough. The second method is the stepwise solver, which creates a solver that uses two computational steps. The first step is the mechanical stationary solver. The result from this step is then used as an initial configuration for the electromagnetic step. However, a problem arises between these two steps, the computation stops. Results indicate that during the mechanical simulation some mesh elements merge together, resulting in the electromagnetic simulation having too many degrees of freedom at the same point to be able to solve the problem. The third method is the fully coupled method. All the computation is done in the same solver, which is in the frequency domain. For each frequency, the mechanics and the electromagnetism are solved together. Therefore the two physics keep track of the changes that are caused by the other. The down side of this method is that the mechanical simulation is recomputed for each frequency, which represents a large penalty in terms of time. Nevertheless the fully coupled method runs without any problem and it is therefore used for the coupling simulation. The reason why this simulation works better than the others is that the moving mesh is automatically used when there is a mechanical simulation.

The fully coupled simulation uses the same geometry as the electromagnetic simulation. In the mechanical part, the only difference between the mechanical simulation alone and the coupling simulation is the incorporation of the air. It is added because the mesh of the air also moves when the aluminum is strained. The mechanical properties of air have to

be added; the Young's modulus is 10^5 Pa and the Poisson ratio is 0. Because the air has a very low Young's modulus, it has a negligible effect on the mechanical part.

The frequency domain solver is used to couple the two physics. For each frequency a stationary problem is solved coupling the mechanics and the electromagnetism. Because the electromagnetism does not influence the mechanical part, the displacement field U and the electromagnetic field E can be solved separately using segregated steps. The first segregated step uses the U field and the second uses the E field. Both segregated solvers use a direct solver to compute the problem. Figure 2.19 shows the S11 for the fully coupled simulation at 1000 με.

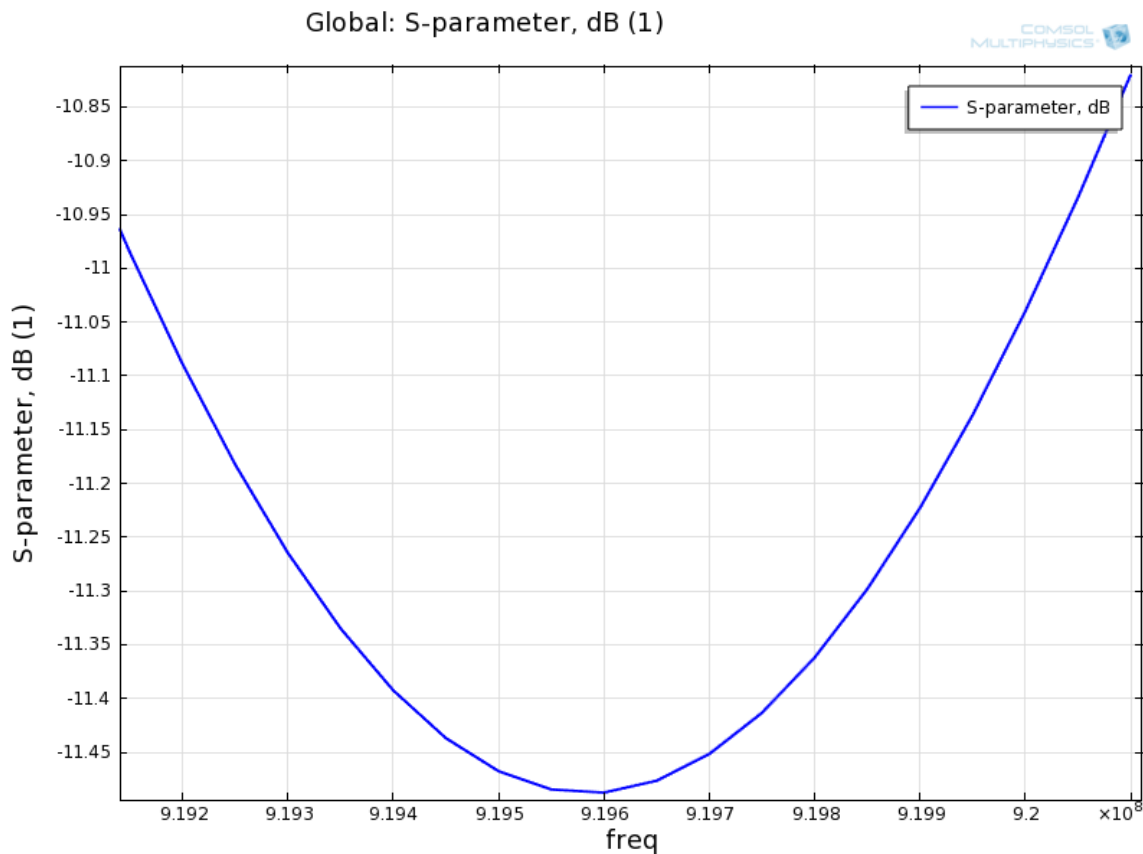**Figure 2.19:** S11 computed by the fully coupled simulation for 1000 με

The shifting is 0.9 MHz, which is a sensitivity of -900Hz/με. This sensitivity is less than the shifting found in Section 2.3.1 times the strain transfer. This result is different from the experimental result, by about 20%. This difference is big enough not to be part of the simulation incertitude. It is suspected that the dielectric constant decreases with increasing strain. This issue will be investigated in future research.

CHAPTER 3

CRACK DETECTION

In addition to strain measurements, the sensor is also investigated for crack detection. This chapter studies the influence of a crack, or large strain concentration, on the sensor. First the sensor is placed next to a crack and the changes in strain are simulated. Simulations varying the planar size and the thickness are conducted in order to give design guidelines for future smaller sensors. The second part of this Chapter presents the experimental results for a crack occurring at the middle of the patch antenna. The simulation of this experiment is shown in the last part.

3.1   Simulation for optimal size and thickness of sensor

A mechanical study has been performed on the crack effect near a patch antenna using COMSOL. The crack is modeled by a rectangular slot transverse to the loading axis (x-axis shown in Figure 3.1). A large strain concentration occurs at the tip of the crack, while strain relaxation occurs along the crack. The crack is placed at the center of the aluminum plate; only a quarter of the plate is simulated for computing efficiency. In order to measure the influence of the crack on the antenna, the antenna patch is placed where the crack produces the largest amount of strain, i.e. the tip of the crack. Exploiting symmetry, only half of the patch antenna is modeled and shown in Figure 3.2. The vias and the matching network are not modeled because they have only a limited effect on the strain on top of the copper.
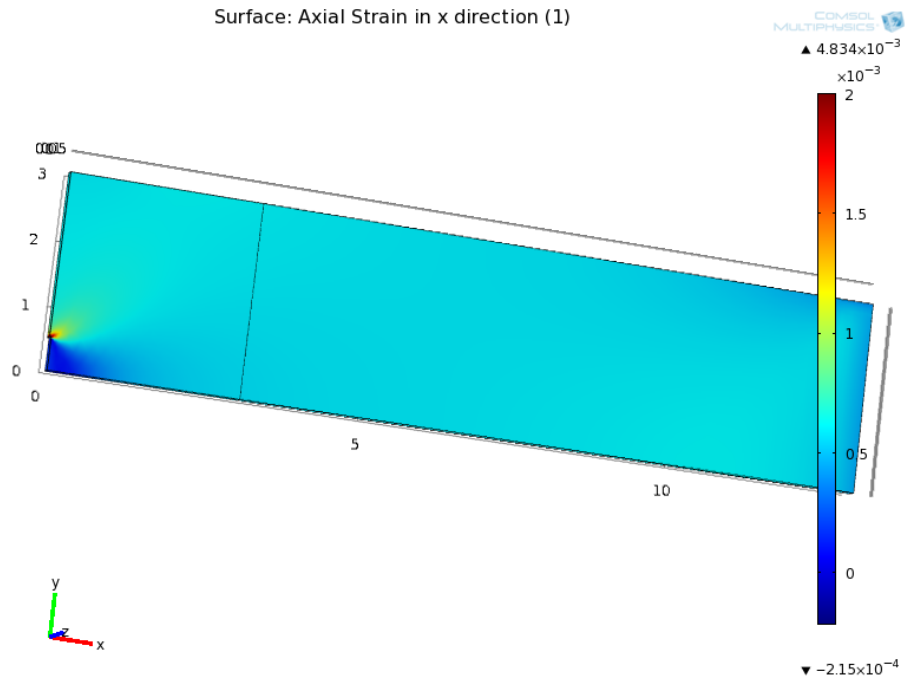
Figure 3.1: Strain in x-axis direction with crack in the aluminum plate (half model)
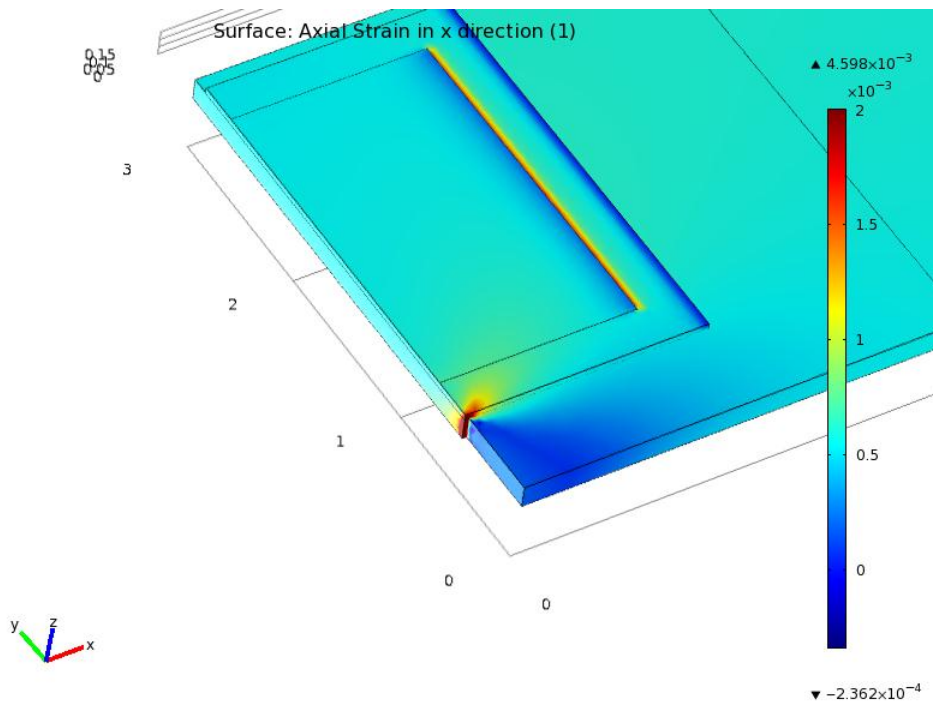

Figure 3.2: Strain in x-axis direction with patch antenna (half patch model) on the

aluminum plate with crack

To characterize the effect of the strain on the patch antenna, two values are observed. The first value is the average strain on the top copper cladding (in presence of the crack) normalized by the same average strain without the crack. The second value is the strain transfer, i.e. the average strain on the top copper cladding divided by the strain in the aluminum (without crack).

3.1.1 Mechanical simulation for patch size

Since crack induced strain concentration is very localized, it only has limited influence on the average strain. The effect of the patch antenna size on the average strain of the top copper layer and on the strain transfer is investigated in this subsection. The plane dimension of the patch (length and width) is changed proportionally while the thickness of the patch remains constant at 31 mils. When the width is 2.4 in, the length is set as 2.7 in (same as the prototype tested in chapter 2).

Figure 3.3 illustrates the top-copper strain ratio of the case with crack over the case without crack, when the plane dimension of the patch antenna is changed. The x-axis of Figure 3.3 is the width of the patch antenna in inches (length changes proportionally). As shown in Figure 3.2, when the plane dimension of the patch antenna decreases, the average strain ratio between the cases with and without crack increases. This means that the existence of the crack has a larger effect on the average strain on the top copper cladding when the plane dimension of the patch antenna is smaller, particularly when the width reduces to less than 0.5 in.

The plane dimension of the patch antenna also affects the strain transfer between the specimen and the top copper layer, as shown in Figure 3.4. The strain transfer is studied using a model without a crack. Figure 3.4 shows the influence of the patch's plane dimension over the strain transfer between the specimen and the top copper layer. The horizontal axis again shows the width of the patch antenna, with its length changing proportionally and its thickness remaining constant as 31 mils. The strain transfer drops

significantly when the patch antenna is smaller than 1-in. in width. These results can be used to guide the design of the next prototype while choosing the optimal dimension to achieve relatively high strain transfer percentage.
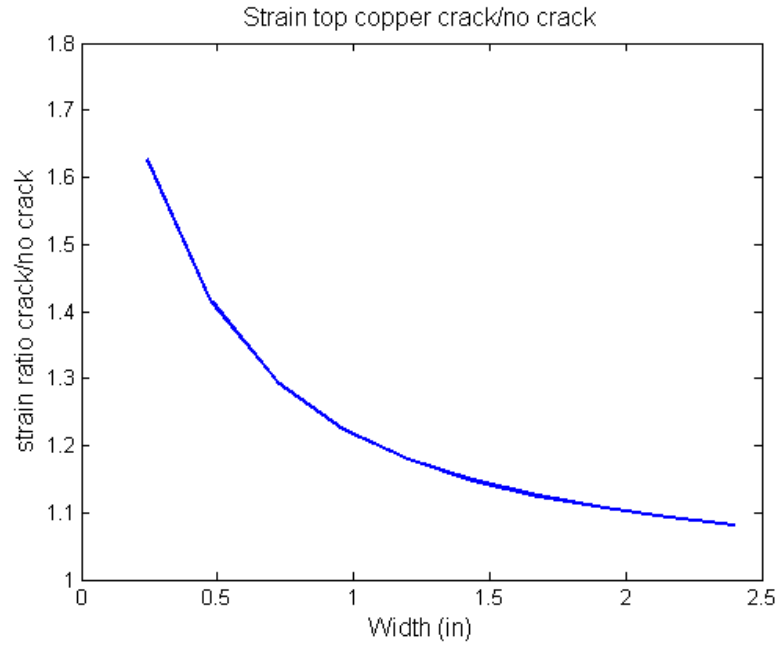

Figure 3.3: Top-copper strain ratio of the case with crack over the case without crack for different plane dimensions
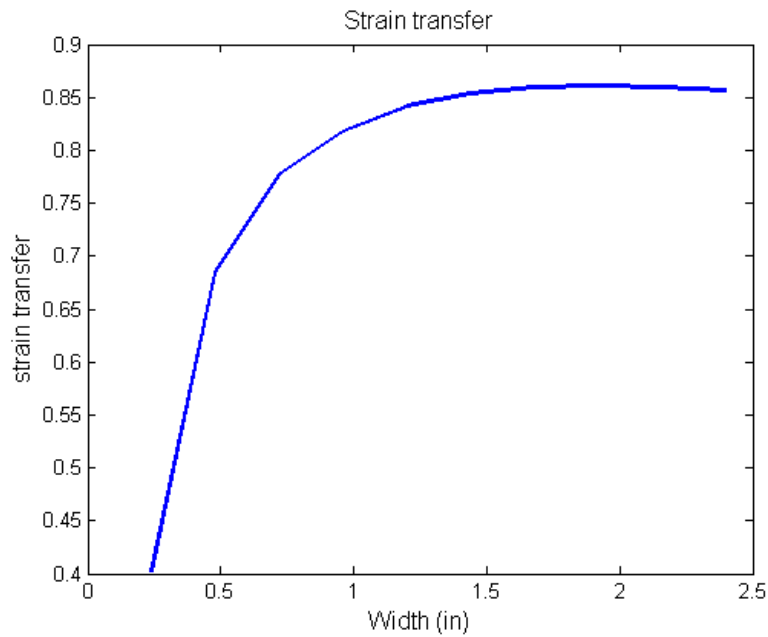

Figure 3.4: Strain transfer percentage for different plane dimensions (without crack)

3.1.2 Mechanical simulation for patch thickness

In addition to the plane dimension, the strain transfer is also sensitive to thickness of the patch antenna. Using a patch of 0.24-in. in width and 0.27 in. in length (i.e. 10% of the plane dimension of the prototype tested), the thickness is reduced gradually from 31 mils to 12 mils, to see its consequence on the strain transfer.

Figure 3.5 illustrates the top-copper strain ratio of the case with a crack over the case without a crack, when the patch thickness is changed (shown by the x-axis). When the thickness of the patch antenna decreases, the average strain ratio between the cases with and without crack increases. This means that the existence of the crack has a larger effect on the average strain when the thickness is smaller.

The thickness of the patch antenna also affects the strain transfer between the specimen and the top copper layer, as shown in Figure 3.6. The horizontal axis again shows the thickness of the patch antenna, while maintaining a plane dimension of 0.24 in. in width and 0.27 in. in length. The strain transfer percentage increases gradually when the thickness is reduced, which confirms thinner substrates provide better mechanical strain transfer.
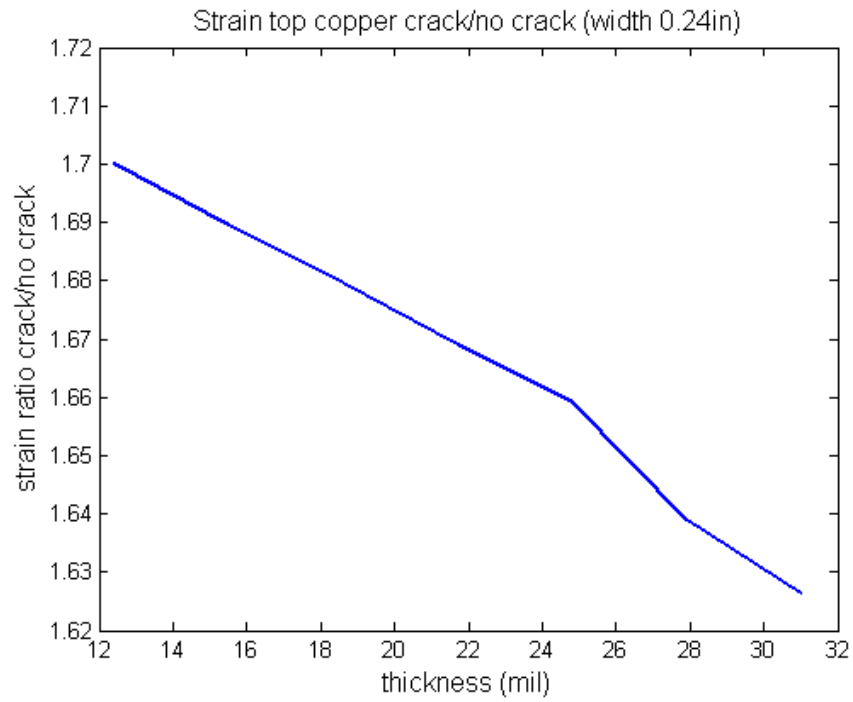
Figure 3.5: Top-copper strain ratio of the case with crack over the case without crack for
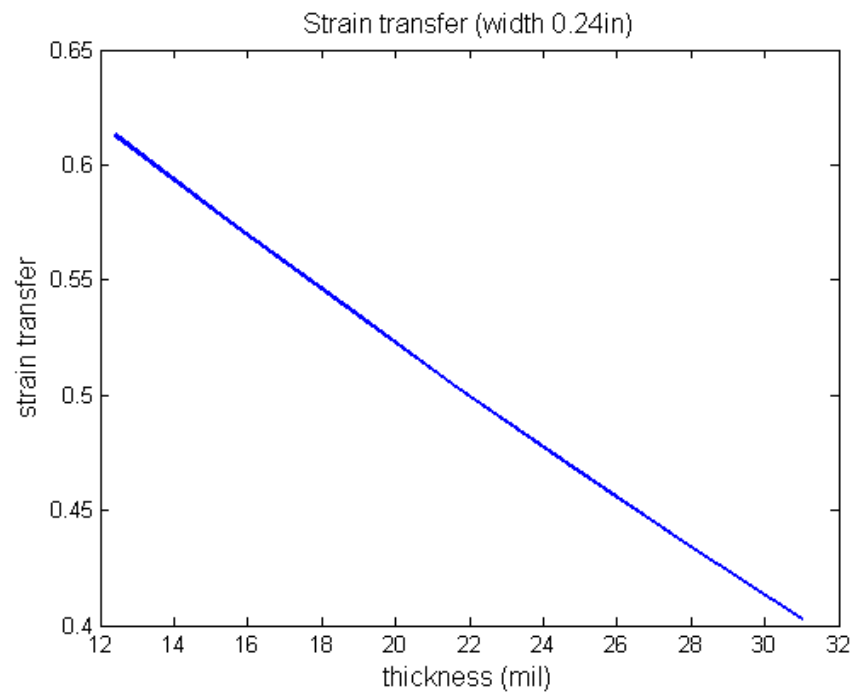
different thicknesses

Figure 3.6: Strain transfer percentage for different thicknesses (without crack)

There is 14% difference of strain between strains when there is a crack and when there is no crack. This small difference could be hard to detect if the accuracy of the sensor is not perfect. There are two ways of improving the sensor: (1) make the sensor smaller so the presence of a crack will induce more strain, (2) use a better estimate of the sensitivity of the sensor.

3.2 Crack sensing experiment

There is a very small difference in strain when the sensor is placed next to a crack. But what happens when the crack passes through the middle of the sensor? This section presents the experimental results for a crack occurring under the middle of the sensor.

3.2.1 Experimental Setup

In order to generate a repeatable and stable crack, a crack testing device is designed and fabricated. Two pieces of 4 in x 8 in. aluminum plates (one rotating and one fixed) are mounted on a 16 in. x 18 in. base plate (Figure 3.7). The thickness of the plates is 0.5 in. The rotating plate can rotate around the axis, producing an opening crack between the rotating plate and the fixed plate. A fine resolution screw controls the opening size, which is measured by a digital dial gauge with a precision of a 0.0001 in.
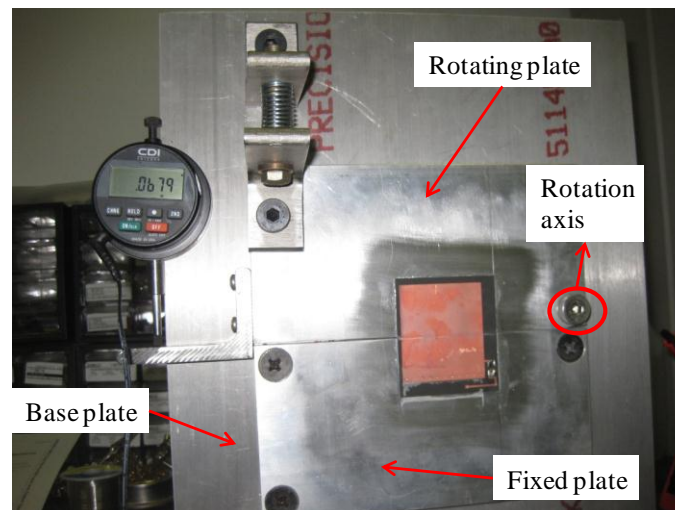

Figure 3.7: Crack testing device for the third Prototype

3.2.2　Crack sensing results

The wireless strain sensor (i.e. patch antenna) is installed at the middle of the opening line between the rotating and fixed plates. The distance between the reader antenna and the crack testing device is set to 12 in. To reduce the effect of measurement noise, a total of five measurements are taken for each crack opening level. After each measurement level, the crack size is slightly increased by turning the control screw for an additional 1/2 revolution.

Figure 3.8 shows the average transmitted threshold for different crack opening sizes as measured at the middle of the patch antenna. The resonance frequency clearly downshifts when the crack opens, and the final recorded decrease is about 6 MHz. After the crack increases to 22 mils (0.56 mm), the patch antenna stopped responding to the reader, and thus, is regarded as damaged. The patch antenna is completely cut into two pieces at 32 mils. Figure 3.9 shows the patch deformation before the patch antenna breaks, while Figure 3.10(a) shows a picture of the sensor just starts to break and Figure 3.10(b) shows a picture of the damage sensor. The crack starts propagating at 22 mils and thus releases tension forces that hold the two pieces of the sensor together. As a consequence, the crack opens even more.
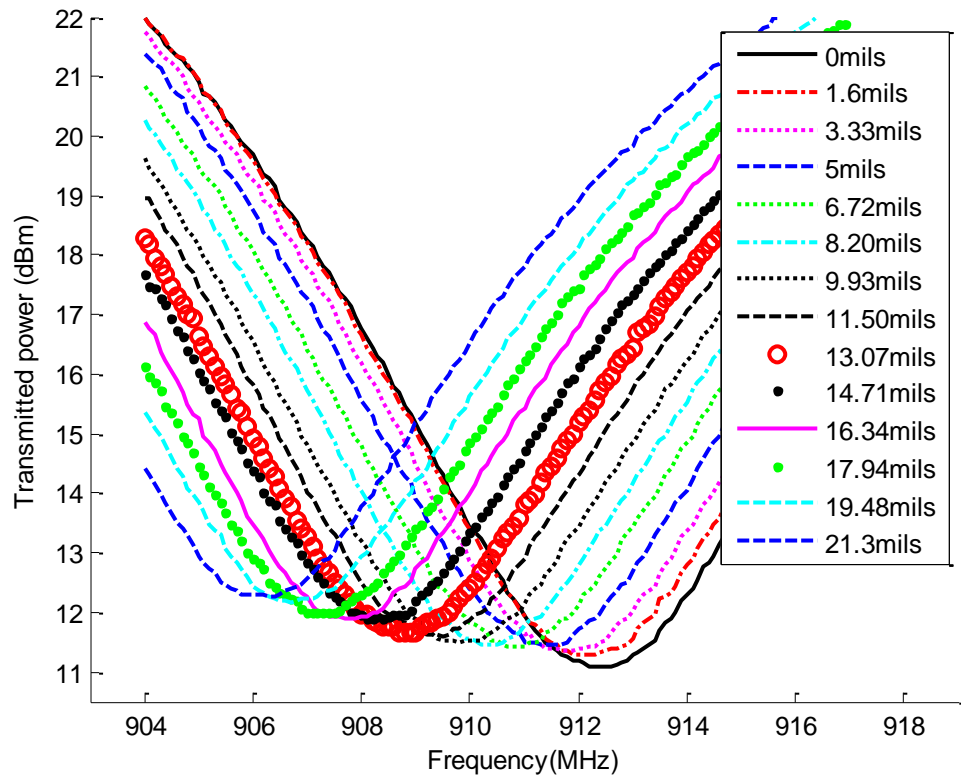
Figure 3.8: Average transmitted power plot for different crack openings
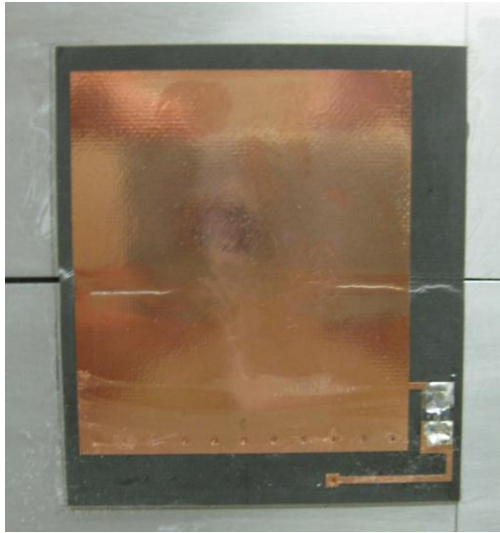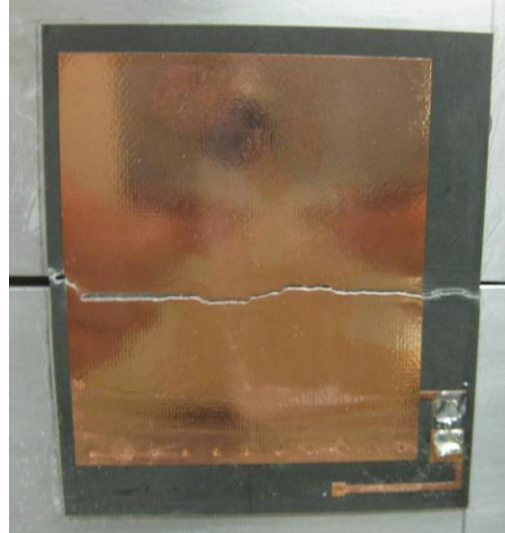

(a) Crack at 9.93 mils

(b) Crack at 19.48 mils

Figure 3.9: Patch deformation before the sensor breaks

(a) Crack at 23.5 mils   (b) Crack at 32 mils

Figure 3.10: Crack testing for the wireless sensor

Figure 3.11 shows the resonance frequency shifts corresponding with the crack size. The resonance frequencies are identified from the valley areas of the transmitted power plots in Figure 3.11. The resonance frequency decreases linearly with a slope of approximately -0.301 MHz /mils. The R^2 is 0.9957, which indicates good linearity of the results. Overall, the experiment illustrates the excellent sensitivity of the wireless sensor for crack detection.
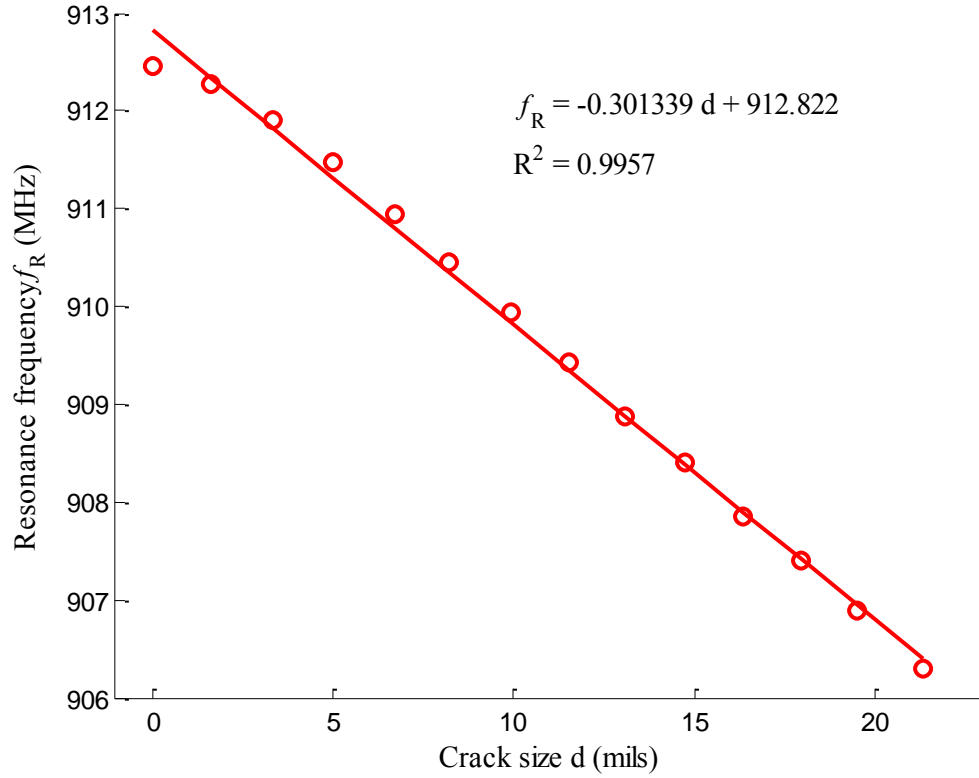
$$f_R = -0.301339\,d + 912.822$$

$$R^2 = 0.9957$$

Figure 3.11: Resonance frequency change (of the patch antenna) versus the crack size

In order to compare the results with typical strain sensing results previously seen, the crack size is divided by the length of the top copper to obtain an equivalent strain. Figure 3.12 illustrates the resonance frequency change with the equivalent strain. The slope is -723 Hz/με, which is in good agreement with the strain sensing results from Figure 2.13. The results from Figure 2.13 are calibrated with the strain transfer but there is no calibration in the results from Figure 3.12. It is hard to measure the strain on top copper in the crack experiment because the strain is very localized. Therefore a simulation is necessary in order to estimate the strain transfer in presence of a crack.
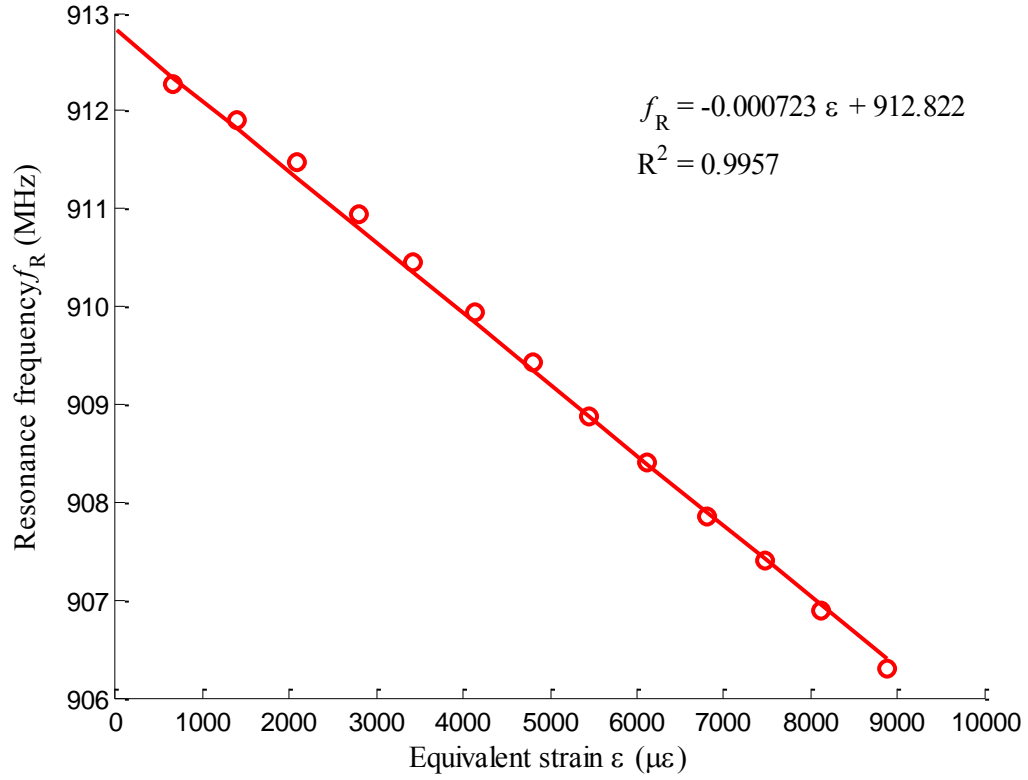
Figure 3.12 Resonance frequency according to equivalent strain

3.3 Crack sensing simulation

The purpose of simulating the behavior of the patch antenna in presence of a crack is twofold. The first purpose is to estimate the strain transfer. The second is to see if the shifting of the resonance frequency can be simulated with a coupling simulation. If the dielectric constant is a function of strain, because the strain is very localized, variation of the dielectric constant will have little effect on the global resonance frequency shifting.

3.3.1 Mechanical simulation

The mechanical simulation uses the same sensor geometry as in Section 2.3. In order to simulate a crack opening, the sensor is placed on top of two aluminum plates. Both plates are 120 mm in width, 82 mm in length and 12.7 mm in depth. In Section 3.2, there is no

crack at the beginning of the experiment. Unfortunately, the mechanical module of COMSOL does not contain functionality for crack simulation. If the two aluminum plates are in contact, they are considered as a continuous solid. Therefore the two plates have to be separated by a preexisting gap. The gap between the two plates is chosen to be 1 mm, because a smaller gap causes the number of mesh elements to increase greatly. Figure 3.13 shows the geometry of the simulation.
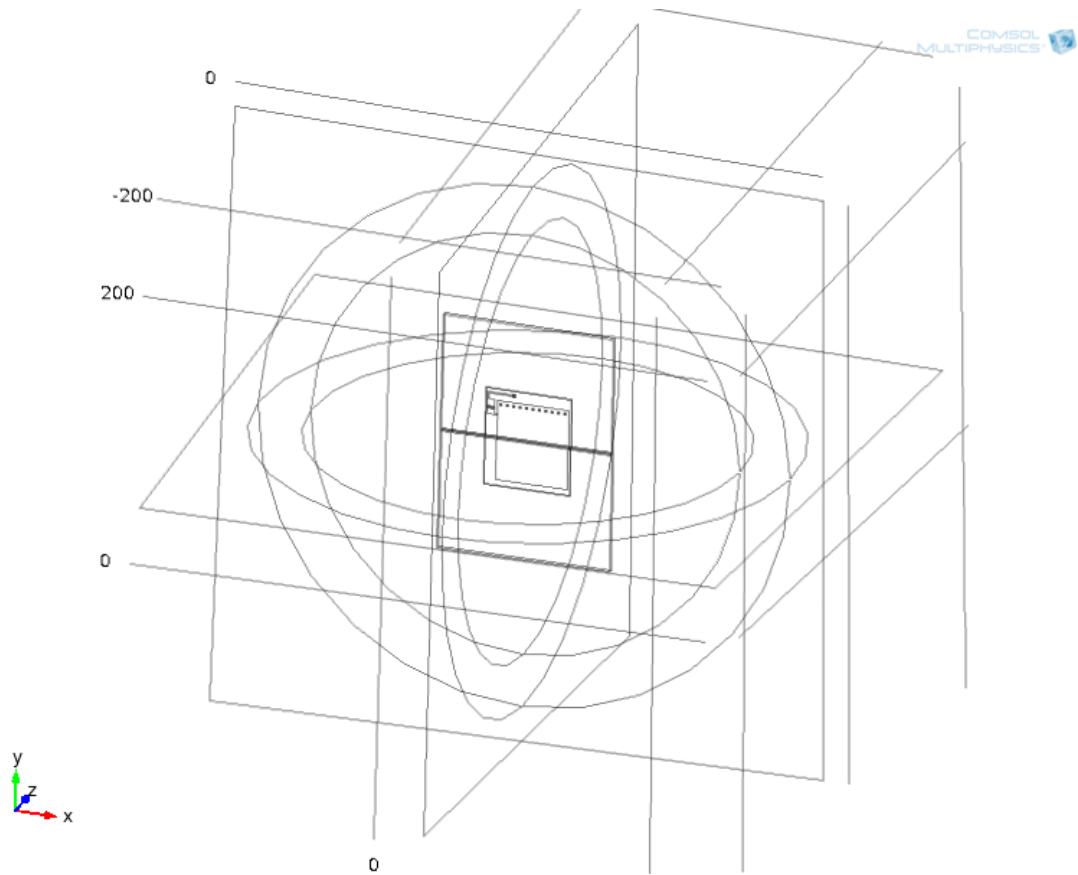

Figure 3.13 Geometry of the mechanical part for the crack simulation

The loading boundary conditions are defined such that the gap increases by 1/1000 of the top copper length, which is the equivalent strain of 1000 με on the top copper. The lower aluminum plate is kept still. A displacement of 1/1000 of the top copper length is applied on the upper surface of the gap.

The meshing and the computing are the same as in Section 2.3.2, using a direct solver to compute the stationary problem. Figure 3.14 shows the strain in the y direction on the sensor and the aluminum plates. The strain is clearly concentrated where the crack opening happens. The average strain on the top copper is 1000 με, which corresponds to an equivalent strain transfer of exactly 100%. A high strain transfer was expected because the displacement is directly applied under the patch antenna and is very concentrated. Nevertheless, the strain transfer in the experiment is probably less because the displacement measurement is not done exactly under the sensor.
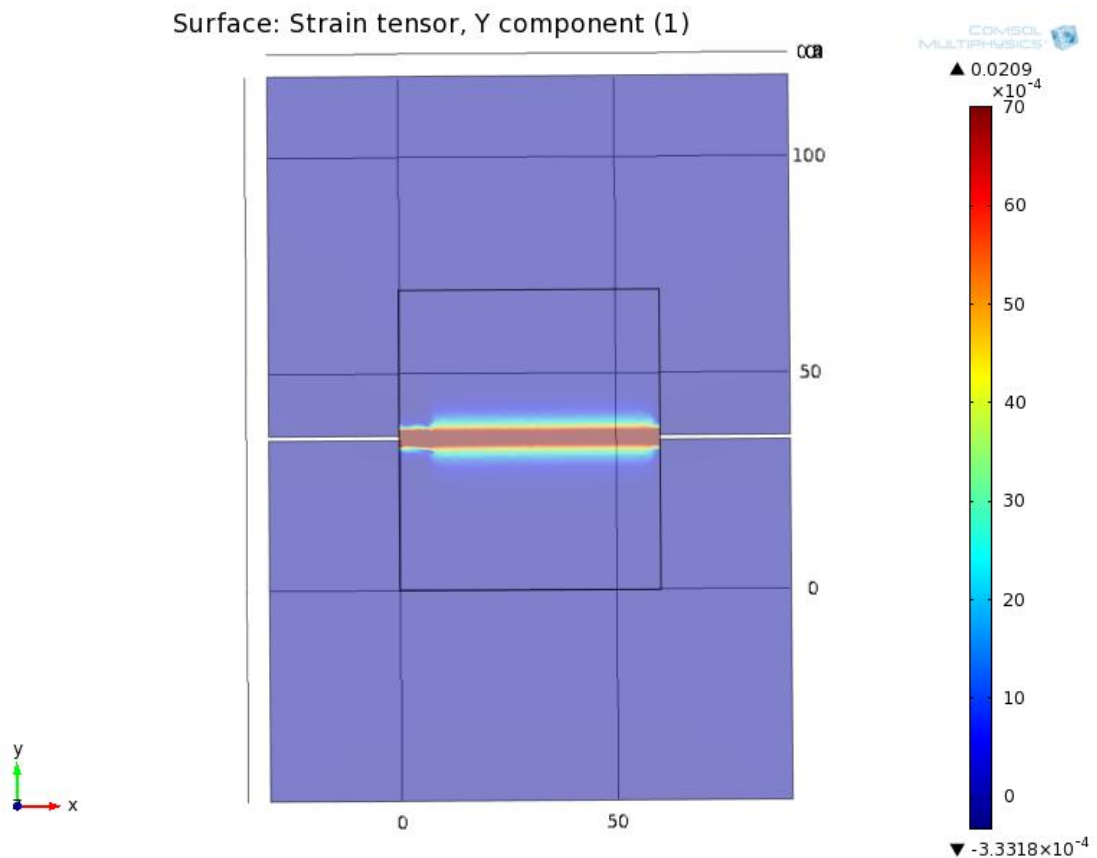

Figure 3.14 Strain in the y direction for the crack simulation

3.3.2 Mechanical-Electromagnetic coupling simulation

The coupling simulation is performed with the settings of section 2.3.3 and the geometry of section 3.3.1. The resonance frequency changes according to the material it is glued on. Therefore the simulation for 0 με is also computed, because the resonance frequency might have changed compared to section 2.3.1. Figure 3.15 shows the S11 at 0 με and Figure 3.16 shows the S11 at 1000 με.

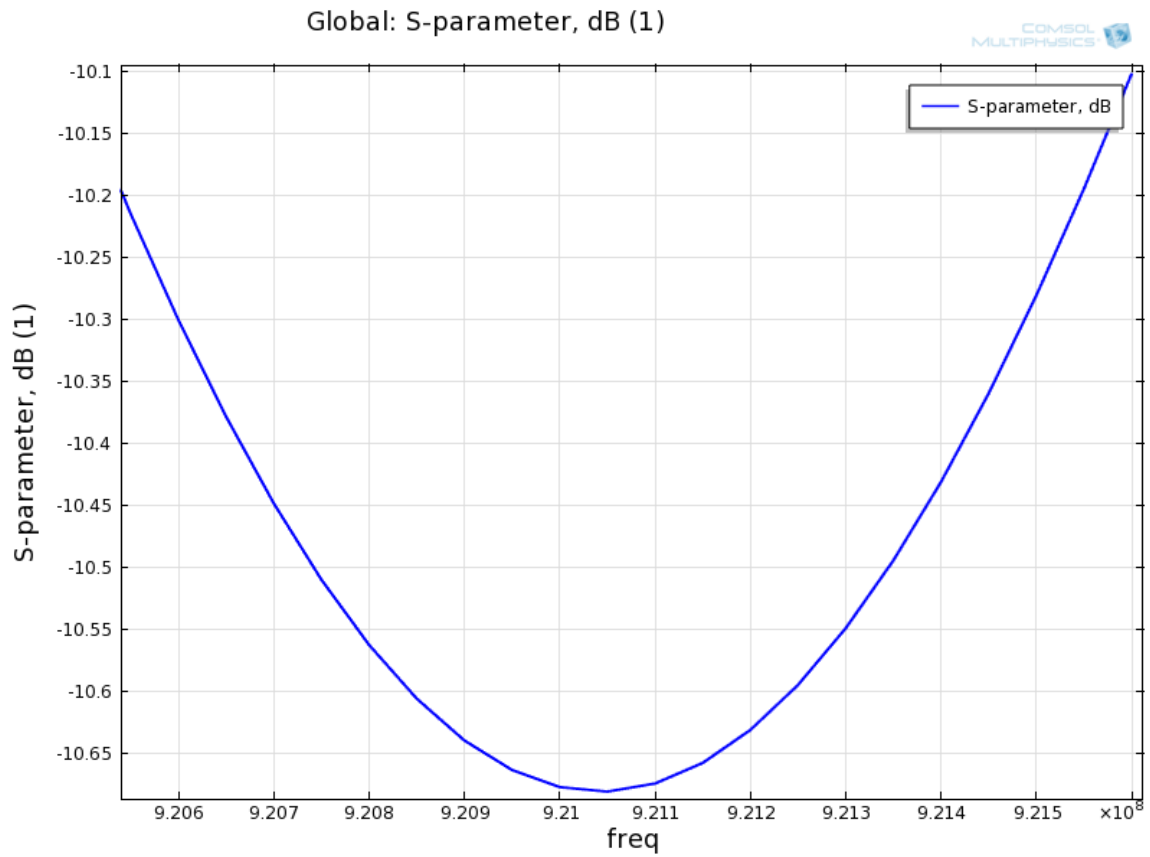**Figure 3.15** S11 for 0 με for the crack simulation
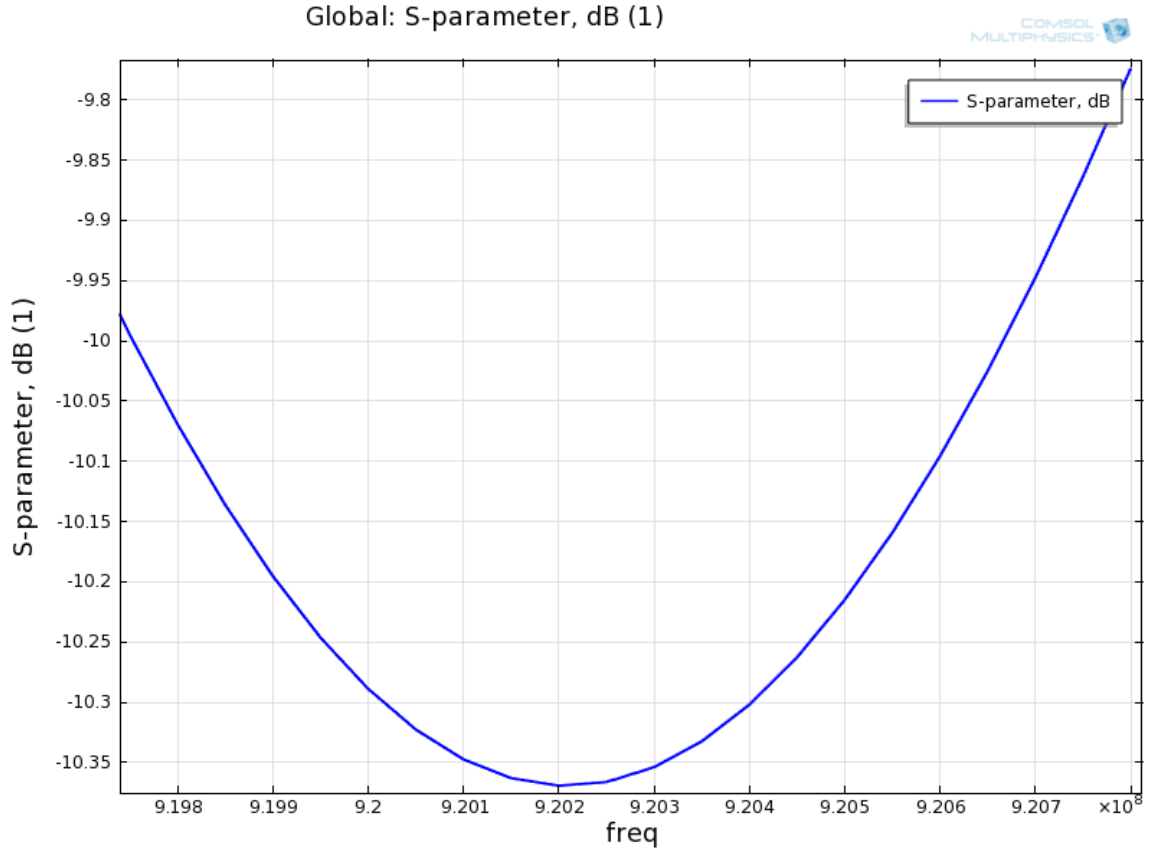
Figure 3.16 S11 for 1000 με for the crack simulation

The resonance frequency at 0 με is 921.05 MHz and at 1000 με is 920.2 MHz. The shift is -850 Hz/με, 6% smaller than the shift for a uniform strain simulated in Section 2.3.3. Although this was not expected, the reason for the smaller shift might be a larger narrowing of the sensor at a localized area. Nevertheless, the difference between the simulation and the experimental result is less than 15%. In the uniform strain experiment the difference of sensitivity between the experiment and the simulation was 22%, much more than in this simulation. Supposing that the dielectric changes according to strain, this change might effect less the crack experiment because the strain is more concentrated and is averaged out. Therefore this explains why the simulation results are closer in the crack experiment than in the uniform strain experiment.

CHAPTER 4

CONCLUSIONS

Finding new technologies to help with crack detection is an important issue for structural health monitoring. Passive wireless strain sensors are a low-cost and innovative solution. RFID technology enables an accurate identification of the sensor and thus allows a large deployment of sensors in small areas. In this thesis we investigated the behavior of a folded patch antenna focusing mainly on the linear relationship between the strain and the resonance frequency (or sensitivity). Simulations coupling electromagnetism and mechanics were performed using the simulation software COMSOL. In presence of uniform strain, the sensitivity is lower than the theoretical calculation and the numerical simulation. This difference is partly due to the strain transfer and a larger part to be studied is the dielectric property change under strain.

The behavior of the sensor near a crack was investigated using both simulation and experiments. Reducing the size and thickness of the sensor would greatly improve the ability of detecting a crack. The performance of the sensor on top of an opening crack is tested. Cracks less than 1 mm can be detected. The sensitivity found for the crack opening is close to the sensitivity in presence of uniform strain after calibration with the strain transfer. No calibration is necessary for the crack case, because the strain transfer is close to 100%. The result for the simulation coupling electromagnetism and mechanics for the crack is closer to the experimental values than for the uniform strain. A change of the dielectric constant according to strain is suspected to play an important role in uniform strain experiment.

This work has studied the sensitivity using a number of hypotheses. The first hypothesis was that the temperature was constant during experiments. A calibration method is described in Appendix A. The second hypothesis was that the glue was perfect and always had the same behavior. In reality the glue changes from experiment to experiment

introducing a large variation in the strain transfer. In the simulations the glue was not modeled. The bottom surface of the sensor was assumed to be perfectly attached to the aluminum. In the simulations a hypothesis was that the dielectric constant does not change according to strain. Using all these hypotheses the sensitivity was investigated focusing mainly on the effect of the mechanical deformation on the resonance frequency. Taking advantage of the progress in simulation software, simulations that couple electromagnetism and mechanics were performed on the current sensor. The results help understanding how the sensor operates in presence of strain.

The difference between the simulation and the experimental results is suspected to be due to a change of the dielectric constant with changes in strain. This variation will be investigated using a microstrip line and loading it at different strain levels. Once the variation of the dielectric constant with strain is known, incorporating it in the coupling simulation will greatly improve the accuracy of the simulation. Future sensor prototypes will be able to use the coupling simulation prior to their fabrication thus estimating the sensitivity. The noise level of the sensor is high. The first method to reduce the noise is by calibrating the results according to the temperature change: initial results are reported in Appendix A.

In order to use these strain sensors in the field, the sensors have to be deployed near strain concentration areas. The position of each sensor has to be optimized to cover an area with a minimum number of sensors. Grid patterns have to be developed to optimize the coverage using the direction and the position of the sensors.

APPENDIX A

THERMAL EFFECT ON THE STRAIN SENSOR

Traditional strain gages are designed to compensate the thermal expansion of the materials they are glued on. The thermal expansion on the wireless strain sensor is much more complex than for traditional strain gages. Firstly the sensor is made of two different materials with different thermal expansion coefficients. Secondly the dielectric constant varies with temperature. This appendix investigates the resonance frequency shift due to the temperature using experimental work.
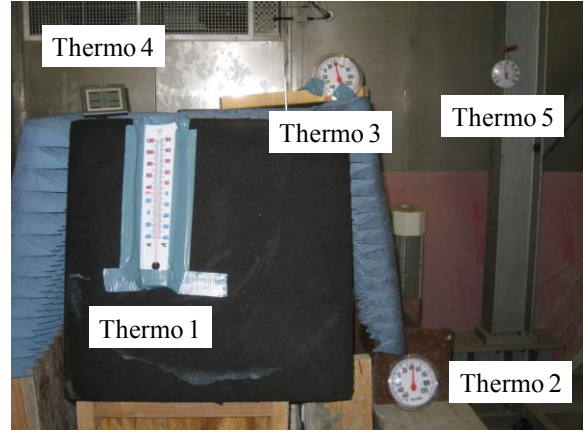
A.1 Experimental setup for temperature test

In order to determine the thermal effects on the strains sensor, the resonance frequency of the prototype sensor is interrogated under different temperatures. The experiment is conducted in an environmental chamber in which the temperature is controlled using a Fast Track 600 from JC Systems.

The sensor is glued on an aluminum specimen and placed at 12 in. away from the reader antenna. Anechoic foams are placed around the reader antenna and the specimen because all the walls of the chamber are covered with metal, which reflect the electromagnetic waves introducing a significant amount of noise. Figure A.1 shows the experimental setup. The chamber is large therefore the temperature inside is not homogenous. Five thermometers are placed inside to measure correctly the temperature.
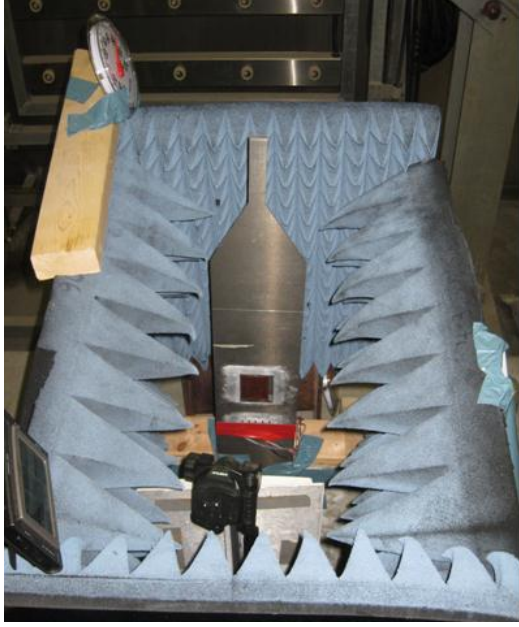
<div align="center">(a) Specimen setup   (b)Thermometer setup</div>

Figure A.1: Experimental setup for the temperature test on the third prototype

A.2 Experimental results for temperature test

The temperature is raised up to 122°F (50°C) and then decreased to 32°F (0°C) at a temperature step of 9°F (5°C°). The ramp time between two temperature steps is 10 min and the soaking time at each step is 20 min. At each step the sensor is interrogated using the transmitted power threshold. Five frequency sweeps are done and then averaged. The transmitted power threshold is plotted in Figure A.2 for average temperature values among Thermo 1 to 4.
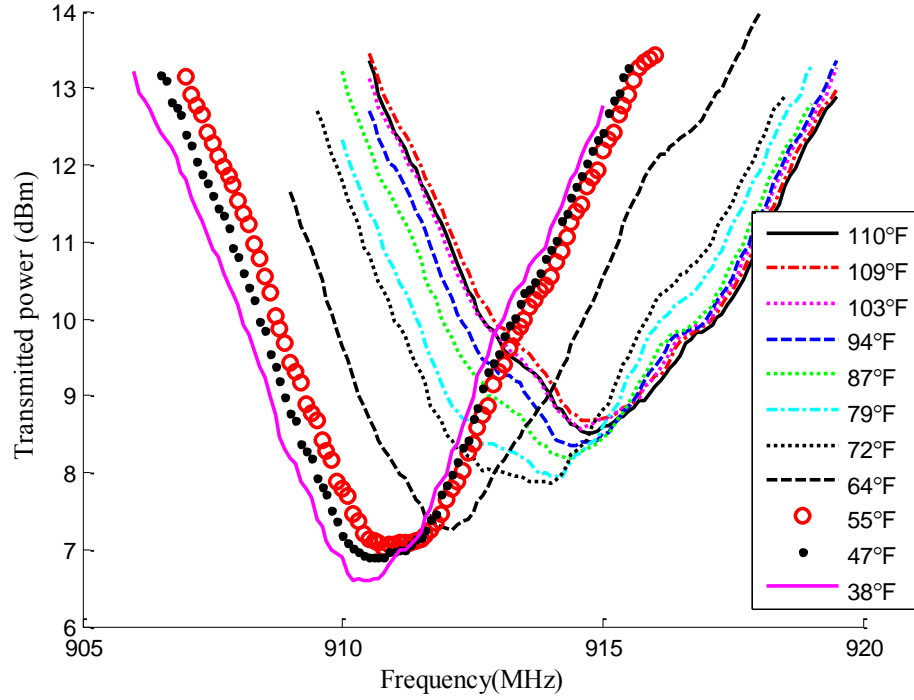
Figure A.2: Averaged transmitted power for different temperatures

The resonance frequency under each temperature is determined by peak picking method after a 4th order curve fitting is performed to the average transmitted power in Figure A.2. The resonance frequency results are shown in Figure A.3 using the average temperature of the thermometers Thermo1, Thermo2, Thermo3, and Thermo4. The resonance frequency shifts more than 4 MHz over a temperature range of 72°F. The equivalent strain corresponding to a shift of 4 MHz using the sensitivity of -700 Hz/με is 5,700 με. Therefore calibrating the resonance frequency shift with its temperature dependence is essential to obtain accurate results.

Two different methods can be used to calibrate the resonance frequency shift. The first method is to measure the temperature next to the sensor using a thermometer. Then correct the shift using the relation between the temperature and the resonance frequency from Figure A.3. The second method is to have a wireless sensor not attached to the structure and use it as a reference for the zero strain resonance frequency. The resonance frequency of this sensor will only shift due to the thermal effect.
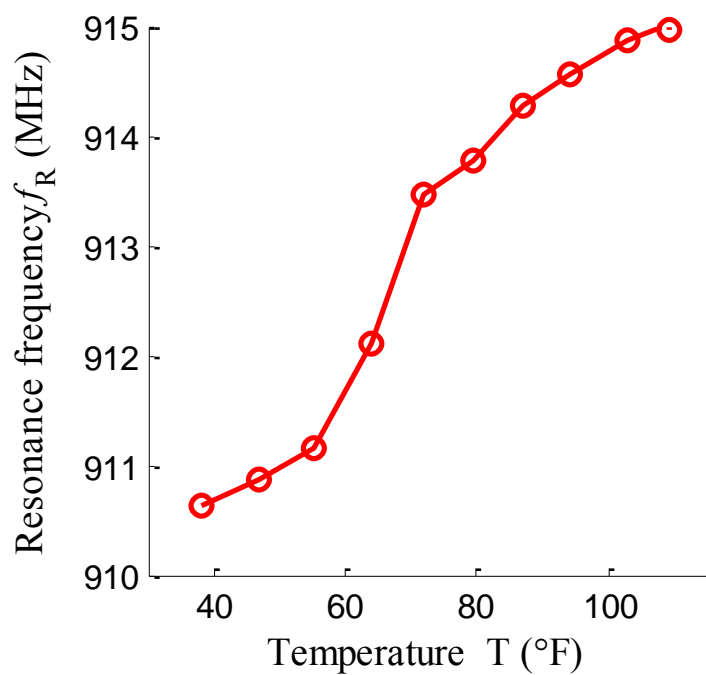
Figure A.3: Resonance frequency captured by peak picking of the transmitted power plot

using the average temperature of Thermo1 to Thermo4

The causes of this large shift are currently being investigated. Two mechanisms occur: (1) the thermal expansion of the materials and (2) the change of the dielectric constant according to the temperature.

APPENDIX B

DIPOLE SIMULATION

In order to test the simulation that couples mechanics and electromagnetism, the simulation of a half-wave dipole under load was conducted. The half-wave dipole is one of the most simple antenna therefore is fairly easy to simulate. The simulation settings are the same as for the simulation in section 2.3.3 but with a different geometry.

The half wave dipole is on top of the Rogers RT/Duroid 5880 substrate. The dimension of the dipole is 303.75x30x0.8 mm. It is feed at the middle by a lump port of 3.75mm wide. Two spheres of radius 240 mm and 300 mm surround the dipole in order to simulate the air. The region between the two spheres is the perfectly matched layer (PML). Figure B.1 represents the dipole geometry.
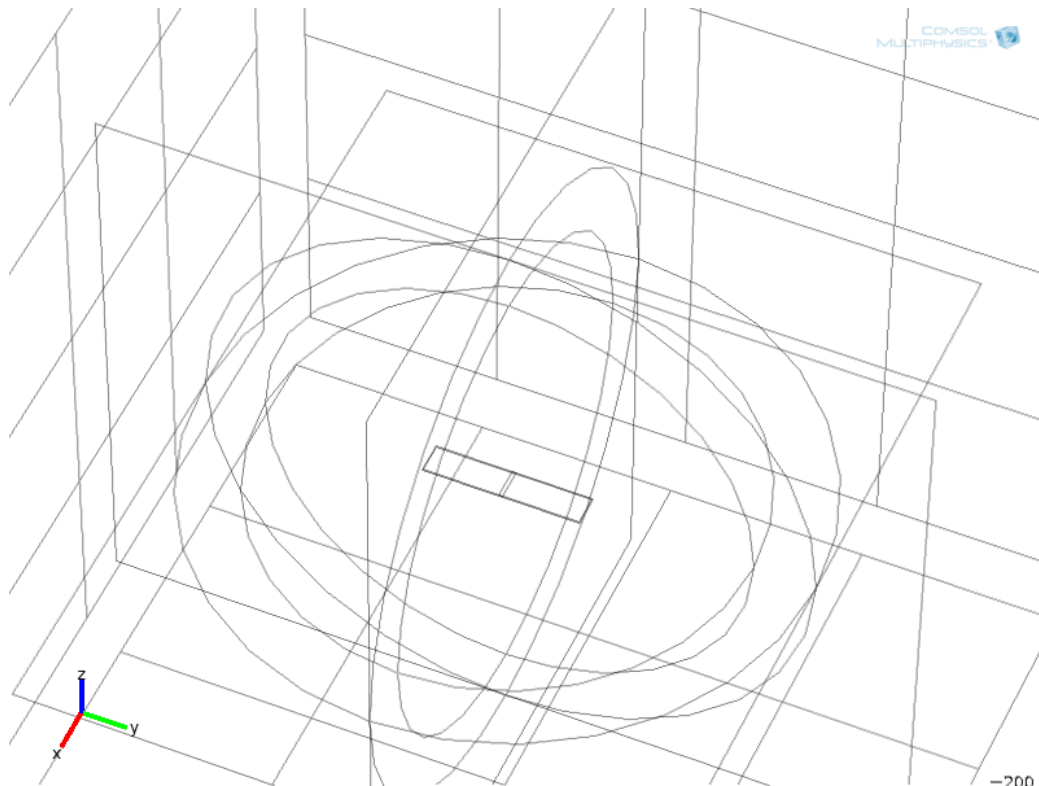

Figure B.1: Dipole geometry

The material used for the dipole is RT/Duroid 5880. The air is modeled using the properties already built-in COMSOL, the Young's modulus and the Poison's ratio for the air are defined as 10^5 Pa and 0 respectively.

The domain between the two spheres is a PML with a spherical wave setting. The top middle surface of the dipole is the feeding port, modeled by a lumped port with a uniform cable excitation of 1V. The lumped port has an impedance of 50 Ohms. A perfect electric conductor models the top surface.

The maximum size of the mesh has to be λ/2 to fulfill Nyquist criteria. The PML is meshed using a swept mesh with quadrilateral elements, insuring a correct absorption of the electromagnetic wave in that region. The rest of the domains are meshed using tetrahedron elements.

In the solid mechanic part, a prescribed displacement is applied at the two ends of the dipole. The displacement chosen is equivalent to 1000με. Figure B.2 shows the strain in the y direction on the dipole for 1000 με. The strain is well distributed along the dipole.
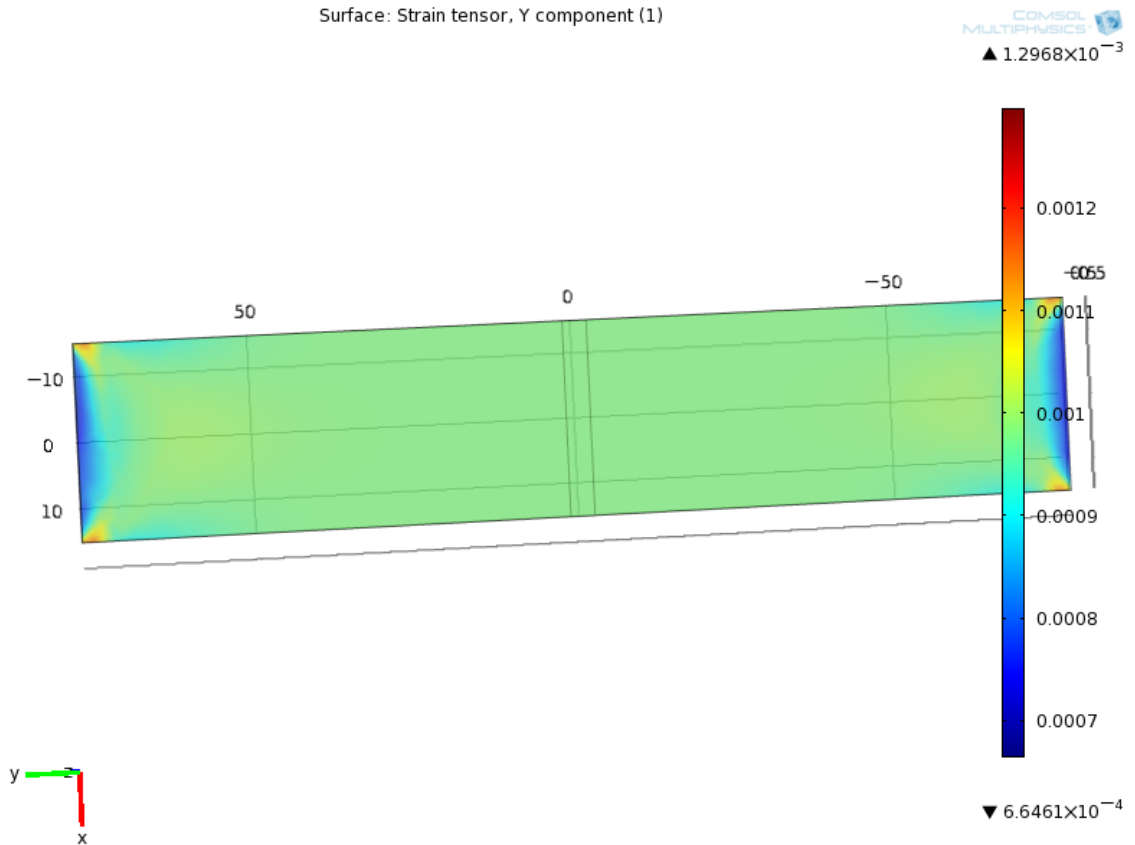
Figure B.2: Strain in the y direction on the dipole for 1000 με

The Frequency domain solver is used to couple the two physics. For each frequency a stationary problem is solved coupling mechanics and electromagnetism. Because the electromagnetism does not influence the mechanical part, the displacement field U and the electromagnetic field E can be solve separately using segregated steps. The first segregated step uses the U field and the second uses the E field. Both segregated solvers use a direct solver to compute the problem. Figure B.3 shows the S11 for 0 με and Figure B.4 shows the S11 for 1000 με.
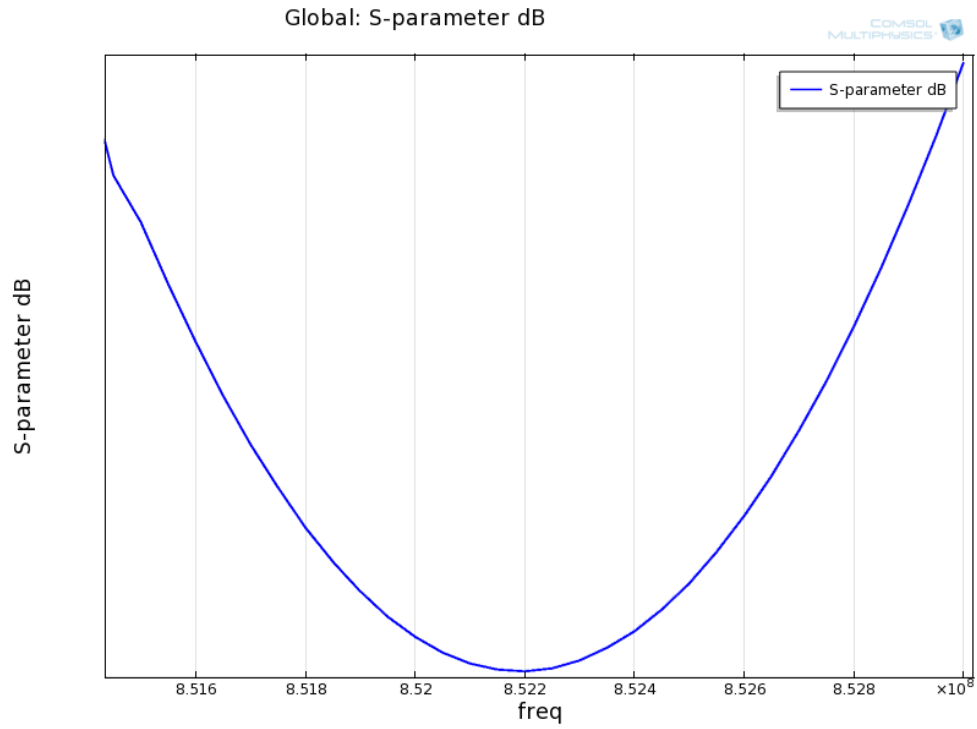
Figure B.3: S11 computed for the dipole simulation for 0 με

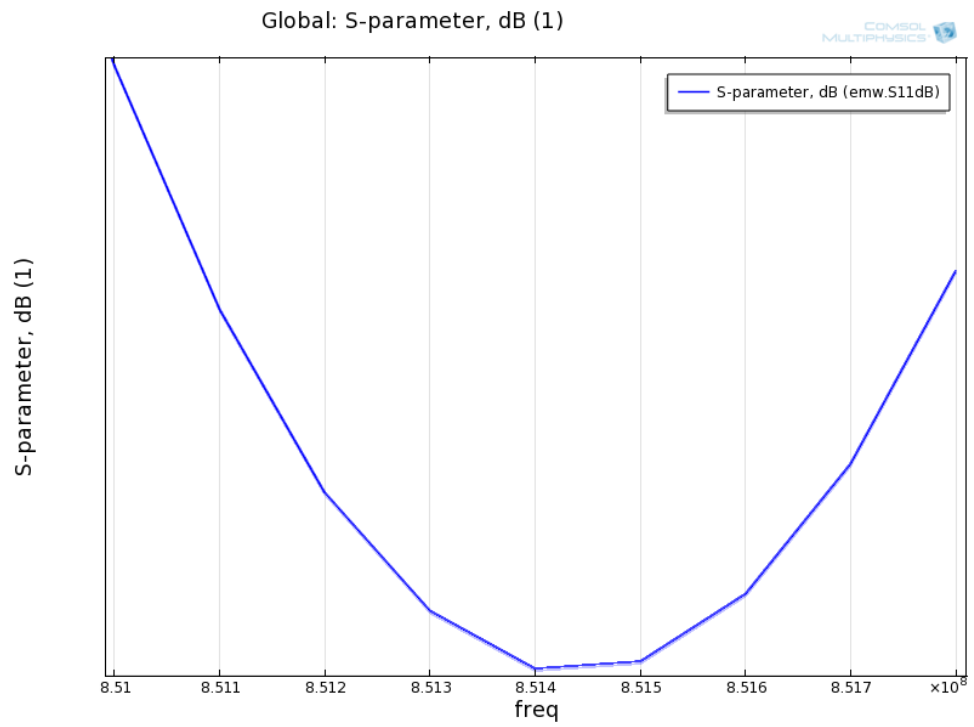**Figure B.4:** S11 computed for the dipole simulation for 1000 με

The resonance frequency shift is -800 Hz/με. The theoretical shifting is -850 Hz/με [20]:

$$f_R = \frac{c}{L(1+\varepsilon)\sqrt{\varepsilon_r}} \qquad \text{(B.1a)}$$

$$\approx f_{R0}(1-\varepsilon) \qquad \text{(B.1b)}$$

where L is the length of the dipole, f_R the resonance frequency, f_{R0} the resonance frequency at 0 με, c the speed of light, ε_r the dielectric constant of the material.

In order to verify the linearity of the shifting, 500 με was applied to the dipole. Figure B.5 shows the S11 for 500 με. The shifting is also -800 Hz/με. This simulation proves that the coupling simulation works well.

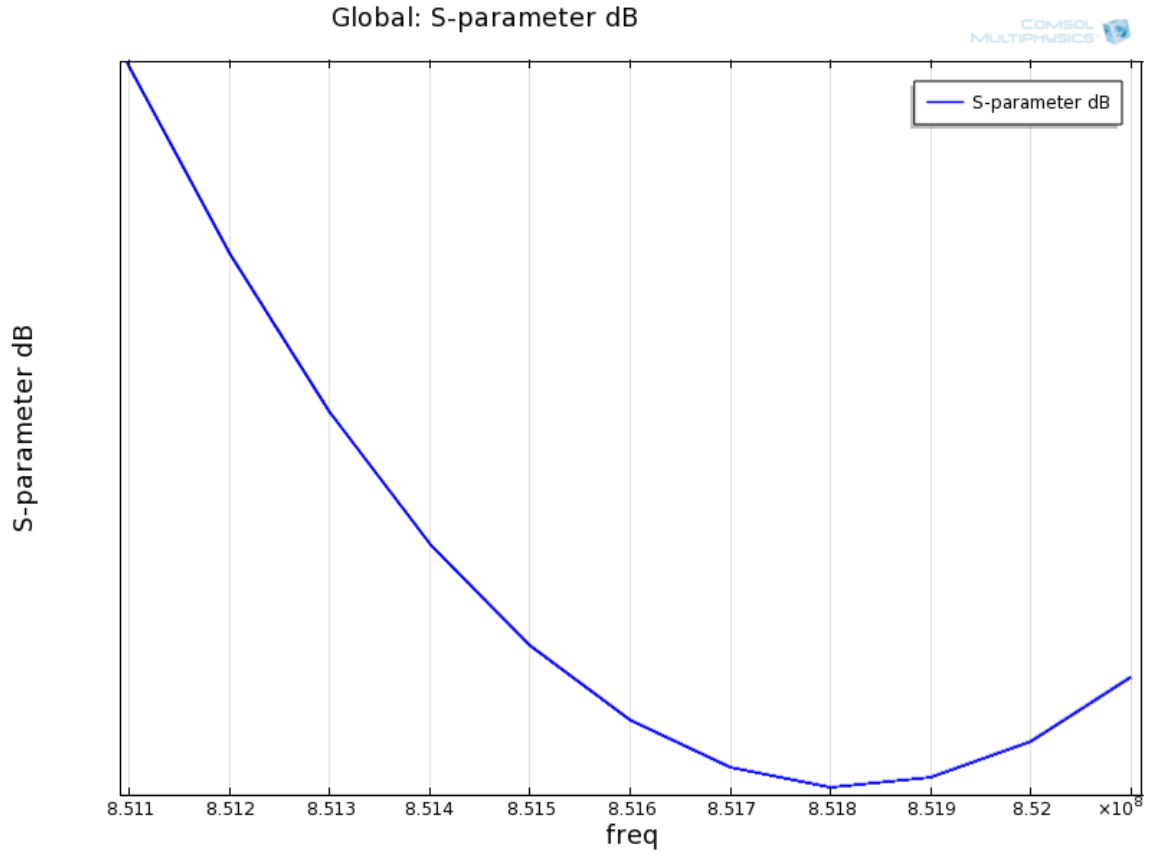**Figure B.5:** S11 computed for the dipole simulation for 500 με

REFERENCES

[1] FHWA. (2011). National Bridge Inventory. U.S. Department of Transportation, Federal Highway Administration, Washington D.C.

[2] Report Card for America's Infrastructure, (2009) American Society of Civil Engineers, Reston, VA.

[3] AASHTO. (2009). Manual of Bridge Evaluation. American Association of State Highway & Transportation Officials, Washington D.C.

[4] Phares, B. M., Washer, G. A., Rolander, D. D., Graybeal, B. A., and, Moore, M., (2004). "Routine Highway Bridge Inspection Condition Documentation Accuracy and Reliability." Journal of Bridge Engineering 9(4): 403-413

[5] Celebi M., (2002). "Seismic Instrumentation of Buildings (With Emphasis on Federal Buildings)," Technical Report No. 0-7460-68170, United States Geological Survey, Menlo Park, CA.

[6] Sazonov, E., Janoyan, K., and Ratan, J., (2004). "Wireless intelligent sensor network for autonomous structural health monitoring." Proc. SPIE 5384(1): 305-314

[7] Lynch, J. P., and Loh. K. J., (2006). "A summary review of wireless sensors and sensor networks for structural health monitoring." The Shock and Vibration Digest 38(2): 91–128.

[8] Doebling, S. W., Farrar, C. R., Prime, M. B., and Shevitz, D. W., (1996). "Damage identification and health monitoring of structural and mechanical systems from changes in their vibration characteristics: A literature review." Los Alamos National Laboratory report LA-13070-MS.

[9] Chuang, J., Thomson, D. J., and Bridges, G. E., (2005). "Embeddable wireless strain sensor based on resonant rf cavities." Review of Scientific Instruments 76(9): 094703

[10] Deshmukh, S., and Huang, H., (2010). "Wireless interrogation of passive antenna sensors." Measurement Science and Technology 21(3): 035201.

[11] Tata, U., Huang, H., Carter, R. L., and Chiao J. C., (2011). "An Antenna Sensor for Crack Detection and Monitoring." Advances in Structural Engineering 14(1): 47.

[12] Merilampi, S., Bjorninen, T., Ukkonen, L., Ruuskanen, P., and Sydanheimo, L., (2011). "Embedded wireless strain sensors based on printed RFID tag." Sensor Review 31: 32-40.

[13] Sample, A. P., Yeager, D. J., Powledge, P. S., Mamishev, A. V., and Smith, J. R., (2008). "Design of an RFID-Based Battery-Free Programmable Sensing Platform." IEEE Transactions on Instrumentation and Measurement 57(11): 2608-2615.

[14] Li, Y., Rida, A., Vyas, R., and Tentzeris, M. M., (2007). "RFID Tag and RF Structures on a Paper Substrate Using Inkjet-Printing Technology." IEEE Transactions on Microwave Theory and Techniques 55(12): 2894-2901.

[15] Anderson, T. L. (1995). Fracture mechanics: fundamentals and applications. 2nd ed. Boca Raton: CRC Press.

[16] Yi, X., Wu, T., Wang, Y., Leon, R. T., Tentzeris, M. M., and Lantz, G., (2011). "Passive wireless smart-skin sensor using RFID-based folded patch antennas." International Journal of Smart and Nano Materials, 2(1): 22 - 38.

[17] Finkenzeller, K. (2003). RFID Handbook. Wiley, New York.

[18] Kutner, M., Nachtsheim, C., Neter, J., and Li, W., (2004). Applied Linear Statistical Models. McGraw-Hill Irwin, Massachusetts.

[19] Pozar, D. M., (2005) Microwave Engineering. John Wiley and Sons Inc., New Jersey.

[20] Balanis, C. A., (1997). Antenna Theory: Analysis and Design. John Wiley and Sons Inc., New Jersey.